High pressure die casting of aluminum alloys: A fluidity-centric review

Zu-nian He[1], Yi-xian Liu[1], Peng-zhan Wang[1], Saria Akhtar[1], Zhi-hong Jia[3, 4], and *Shou-mei Xiong[1, 2]

1. School of Materials Science and Engineering, Tsinghua University, Beijing 100084, China

2. Key Laboratory for Advanced Materials Processing Technology, Tsinghua University, Beijing 100084, China

3. Key Laboratory for Light-Weight Materials, Nanjing Tech University, Nanjing 211816, China

4. Yangtze Delta Region Institute of Advanced Materials, Suzhou 215000, Jiangsu, China

Abstract: Fluidity is one of the critical indicators for evaluating castability and has become a major research focus over the past five years due to advancements in high pressure die casting (HPDC) technology. Aluminum alloys, which were widely used in HPDC, offer promising structural and functional properties. The variables affecting the fluidity of alloy determine the solidification mode and the behavior of liquid flow, which forms the fundamental basis for understanding and controlling the macroscopic flow length. Here, an up-to-date and comprehensive review of research on fluidity of HPDC aluminum alloys is provided. It begins by discussing the main variables affecting fluidity, such as shot phases, compositions, solidification mode, and flow regime transition. The discussion then presents a summary of the recently proposed flow choking mechanisms. Additionally, algorithms related to fluidity under HPDC are reviewed, with particular emphasis on the increasing application of machine learning techniques in recent years. Finally, remaining challenges and perspectives for future materials, processes, and applications in HPDC fluidity research are proposed.

Keywords: fluidity; high pressure die casting; aluminum alloys; models; algorithms

CLC numbers: TG146.21 **Document code:** A **Article ID:** 1672-6421(2026)04-485-30

1 Introduction

High pressure die casting (HPDC) is a traditional processing method to manufacture complex thin-walled castings[1]. Recent advances in HPDC equipment have aroused interest in the research of process parameters and melt flow behavior. The flow pattern[2] and alloy composition[3] are regarded as key factors in material design and performance iteration. Aluminum (Al) alloys have long been fundamental in industries requiring lightweight[4], high strength[5], high thermal conductivity[6], and corrosion-resistant[7] materials, which had been combined with the HPDC process for decades. In 2022, cast Al alloys account for 65.9% of Al alloys used in North American electric vehicles (EVs)[8]. The utilization of Al alloys in automotive manufacturing is progressively rising each year.

The explanation of fluidity in HPDC fields was first promoted by Flemings et al.[9] in 1963. It is defined as the maximum flow length reached by the alloy before solidification halts its movement. Importantly, fluidity cannot be simply equated to the reciprocal of viscosity. Recent advancements in integrated die casting technology[10] have deepened the understanding of fluidity, enabling more precise control of the fluidity characteristics of Al alloys. Over nearly five years of research, the complexity of modeling flow behavior under HPDC conditions has significantly advanced. Research has progressed from examining the impact of individual variables on fluidity to investigating the combined influence of various casting variables (e.g., slow and fast shot speeds[11-15]) and metallurgical variables (e.g., alloy composition, superheat, latent heat, and solidification mode[16-19]). Additionally, the combined effects of flow patterns and heat transfer on fluidity have become a focal point of study[20]. Researchers have developed various analytical models to predict maximum flow length and filling time, ultimately progressing to use flow choking mechanisms[19] and machine learning (ML) algorithms

*Shou-mei Xiong

Male, Ph. D., Professor. Research interests: Al and Mg alloy high pressure die casting and microstructure simulation during solidification.

E-mail: smxiong@tsinghua.edu.cn

Received: 2025-03-16; Revised: 2025-08-20; Accepted: 2025-09-08

for predicting fluidity and defect formation[21]. This evolution in research reflects a trend toward more comprehensive and in-depth exploration of fluidity in HPDC.

Unlike gravity casting that involves relatively lower complexity in die design and reduced gate speed, HPDC simultaneously enhances die complexity and gate speed. This results in a layered microstructure within Al alloys, characterized by a core of externally solidified crystals (ESCs), defect band, and outer skin layer[22, 23]. The formation of this layered structure is primarily driven by shear localization and difference of cooling rates[24]. Due to the slower heat dissipation within the core and the presence of ESCs in the shot sleeve, achieving a stable, fine-grained, equiaxed structure in the core region remains challenging. However, the diversity of process parameters and elemental selection offers substantial potential for microstructure-property optimization[25]. This research aims to identify the critical factors influencing fluidity, and thus facilitating a controlled HPDC process. Despite extensive research, the impact of variables (including casting variables, metallurgical variables, and flow variables) on solidification mode and fluidity remain inadequately understood. To systematically investigate fluidity under HPDC conditions, a comprehensive and in-depth understanding of the relevant variables and model development mechanisms is essential. Summarizing and analyzing the contributions of previous research works in this field will establish a methodological framework that guides future studies.

In recent years, extensive research on HPDC technology has produced insightful reviews, with growing focus on gating system design, alloy composition, process parameters, and solidification mechanisms[10, 26]. Reviews of Al casting alloys often emphasize mechanical properties and thermal conductivity[27, 28]. In contrast, this review aims to summarize the latest research progress on the fluidity behavior of Al alloys under HPDC conditions, with a particular focus on the influencing variables. The discussions include three aspects: variables, flow choking mechanisms, and algorithms. Both theoretical and experimental findings are examined to offer insights into recent advancements.

2 Variables affecting fluidity

2.1 Casting variables

Generally, there are three critical process parameters that significantly influence fluid filling during the slow shot phase, fast shot phase, and intensification pressure (IP) phase. These parameters are primarily determined by the settings on the die casting machine. Additionally, fluidity is also influenced by gating ratio, die parameters (include temperature, material, coating, and permeability), and die shape, which are determined by the die. The following discussions will delve into the reasons for the impact of these variables on fluidity, detailing the specific effects of each parameter and exploring their mechanisms.

2.1.1 Slow shot phase

The stability of flow and vacuum time in HPDC is influenced by the slow shot phase including slow shot speed and slow shot position [Fig. 1(a)]. Controlling the slow shot speed and its position can reduce air entrapment and ensure vacuum integrity[29]. During the slow shot phase, molten metal is introduced into the die cavity at a controlled speed, which significantly influences the formation of ESCs and the risk of gas entrap. Excessive slow shot speeds can lead to air entrapment[30], whereas insufficient speeds may induce premature solidification[31] and incomplete cavity filling[32]. These conditions promote porosity formation in the metal front upon solidification[33]. An increased slow shot speed has been shown to increase the porosity volume fraction and modify the primary particle size distribution, thereby impacting the final casting fluidity[11].

Nikroo et al.[14] analyzed the flow behavior of molten metal in the shot sleeve during the slow shot phase by using a 3D numerical model based on the finite difference method and the volume fluid method. The wave velocity and plunger velocity in a shot sleeve with a rectangular cross-section can be written as:

$$\begin{cases} V_w = \dfrac{T}{T-D} V_p \\ V_p = (T-D)\sqrt{\dfrac{2g}{T+D}} \end{cases} \tag{1}$$

where V_w and V_p represent the wave velocity and plunger velocity, respectively, T is the depth of fluid behind the wave in the shot sleeve, D is the depth of fluid in front of the wave in the shot sleeve, and g is the gravitational acceleration.

This model focuses on the melt flow dynamics and air entrapment within the shot sleeve, which can significantly impact casting quality. Key parameters, such as plunger velocity, acceleration, and the geometry of chamber, influence the risks of air entrapment during die filling. Specifically, acceleration has a direct effect on waveform stability of melt flow during injection [Fig. 1(b)]. Increased acceleration tends to reduce the wave thickness, thereby promoting its stability, while inadequate acceleration can lead to wave breaking. Compared to circular shot sleeves, rectangular cross-sections reduce wave rolling (V_W) and the associated air entrapment (V_P), which is expressed as follows:

$$\begin{cases} V_w = \dfrac{\beta}{\beta-\phi} V_p \\ V_p = \sqrt{2g\dfrac{(T-D)(\beta-\phi)}{\beta+\phi}} \end{cases} \tag{2}$$

where β is the proportion of the shot sleeve cross-sectional area filled with fluid behind the wave, and ϕ is the proportion of the shot sleeve cross-sectional area initially filled with fluid[34].

The critical plunger speed[35] is the slow shot speed that lifts the wave caused by the plunger movement to the highest point without causing the wave to roll [Fig. 1(c)]. Combining the shallow-water theoretical modeling with numerical simulations [Fig. 1(d)], this study assesses several plunger acceleration laws. The findings suggest that a formulated exponential, time-dependent acceleration law is most effective at reducing air entrapment. This law minimizes wave reflection and prevents premature wave breaking within the shot sleeve, thereby mitigating the risk of porosity in cast components. Kohlstädt et al.[36] used computational fluid dynamics method (in the form of OpenFORM) to model the complex flow behavior in the shot sleeve during the slow shot phase of plunger motion. The simulation focused on determining the critical plunger speed, with results closely aligning with analytical models derived from shallow-water equations.

For microstructure, as the slow shot speed increases, the average size of primary Si decreases in Al-Si alloy[37]. Similarly, as the slow shot speed increases, both the size and quantity of ESCs and pores are reduced, effectively eliminating the net-shrinkage microstructure [Figs. 1(e) and (f)]. Additionally, the distribution of ESCs becomes more dispersed throughout the casting samples, leading to improved material uniformity and reduced defect concentration[12]. A multi-step slow shot speed approach reduces both the dwell time of melt in the shot sleeve before die filling and the initial vacuum pressure within the die cavity[13]. Setting a higher slow shot speed in the early phase minimizes the dwell time of Al alloy in the shot sleeve, while a lower slow shot speed in the later phase can form a stable waveform and maintain an appropriate vacuum duration.

In summary, the slow shot phases help efficiently evacuating air, reducing defects, and improving the quality of castings. Among reported research results, a higher slow shot speed decreases the time spent in the shot sleeve and reduces the number of ESCs, which may delay the creation of mushy areas in the flow path and increase fluidity.

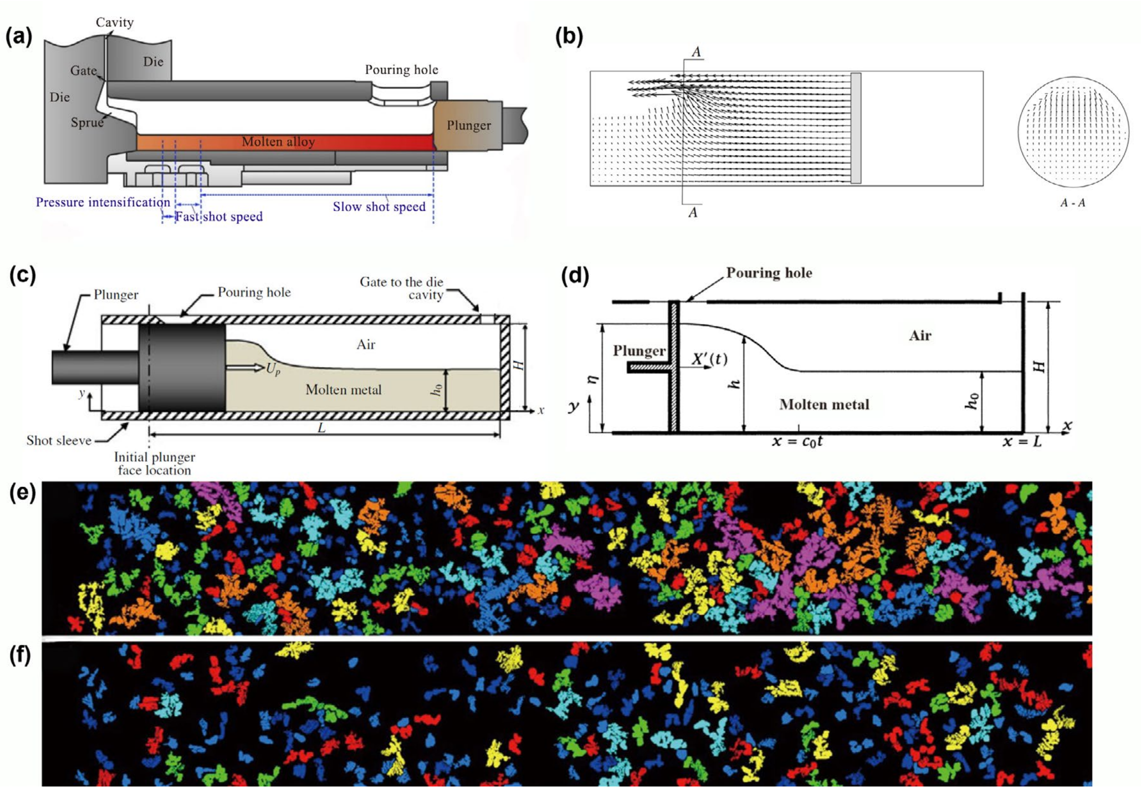

Fig. 1: Slow shot phases in the shot sleeve driven by the plunger of a HPDC machine, showing fluid dynamics and ESC distribution under varying speeds: (a) initial condition before plunger movement[11]; (b) flow vector diagram at the start-up phase[14]; (c, d) fluid flow models at slow shot phases[35, 36]; (e) ESCs distribution at a slow shot speed of 0.1 m·s^{-1} [12]; (f) ESCs distribution at an increased slow shot speed of 0.4 m·s^{-1} [12]

2.1.2 Fast shot phase

The metal is introduced into the die cavity at high velocities, generally ranging from 20 to 80 m·s^{-1}[38, 39], under elevated pressure conditions. As demonstrated in Fig. 2(a), the theoretical gate speed exhibits a proportional relationship with the fast shot speed, expressed as gating ratio, Ω. The fast shot phase determines the shape of the liquid flow from the shot sleeve into the die. Different shapes directly influence the development of turbulence in the die[40], thereby affecting the flow length. The fast shot phase has been recognized as a critical factor impacting fluidity in HPDC, however, research in this area remains limited. Recent studies have started to examine the shear forces of fluid flow exerted by the die-filling process[24], as well as the volume fractions of pores and ESCs[15, 41, 42].

The fast shot speed determines the intensity of the flow shear, which in turn affects the distribution and the spheroidization level of ESCs. The injection process decreases the content of floating crystals in the mixture at the start of die filling, preventing the formation of an ESCs dendrite network at gate cross-sectional transitions. Higher fast shot speed helps maintain metal fluidity by mitigating early-stage flow obstructions[24, 31]. The highest value of fluid shear stress was reached when the fluid flowed through the gate with the highest speed during the injection. As a result, agglomerated particles formed during stirring could be effectively dispersed by the fluid shear during the HPDC die filling process, and form a shearing zone along the flow direction [Fig. 2(b)], leading to a uniform distribution of particles within the matrix[43]. According to the Prandtl fluid mechanics[44] and the multiphase flow theory[45], the fluid shear can be assessed.

Xie et al.[15] investigated the influence of increased fast shot speeds in HPDC on the microstructure and mechanical properties of Mg-Al-Zn-RE alloys. The study indicates that higher shot speeds promote finer, more uniform grain sizes, reduce the area fraction of ESCs [Fig. 2(c)]. The same result was found in AlSi10MnMg alloy [Fig. 2(d)] and porosities were also decreased[41]. Additionally, the smaller grain sizes enhance the overall grain structure beyond ESC reduction. The increased shot speed leads to the breakup and homogenization of ESCs, creating more nucleation sites during solidification, which supports fine-grain strengthening and enhances mechanical properties. Current literature reports conflicting results, showing that grain refinement can both increase and decrease fluidity. Therefore, it remains unclear whether fluidity is related to grain refinement itself or the refinement method. This will be further discussed in Section 2.2.1.

When the fast shot speed is low (1 $m \cdot s^{-1}$), the flushing action of the melt on the die wall is weak, and the die temperature rises less during the filling process. This results in a large temperature difference between the melt and the die wall, leading to the formation of a thick skin layer with a high density of chilled crystals[46]. As the fast-shot speed increases, the melt flow velocity during die filling also increases, intensifying the erosion (or flushing) effect on the die walls[30]. This causes a sharp rise in the die wall temperature and a significant reduction in the temperature difference between the melt and the die wall, thereby decreasing the number of chilled crystals and the thickness of skin layer [Fig. 2(e)]. The skin layer tends to push particles away from the wall towards the sample interior, resulting in fewer particles in the skin layer. This indicates that the Magnus effect dominates at lower fast shot speeds, while increasing the fast shot speeds makes the turbulence effect dominate, promoting uniform distribution of solids. Besides, the skin layer has negative effects on the compressive and corrosion resistance, airtightness, machining, and mechanical properties of HPDC products.

In addition to experimental observation of solidification structure, a hybrid finite element mesh can also be used to

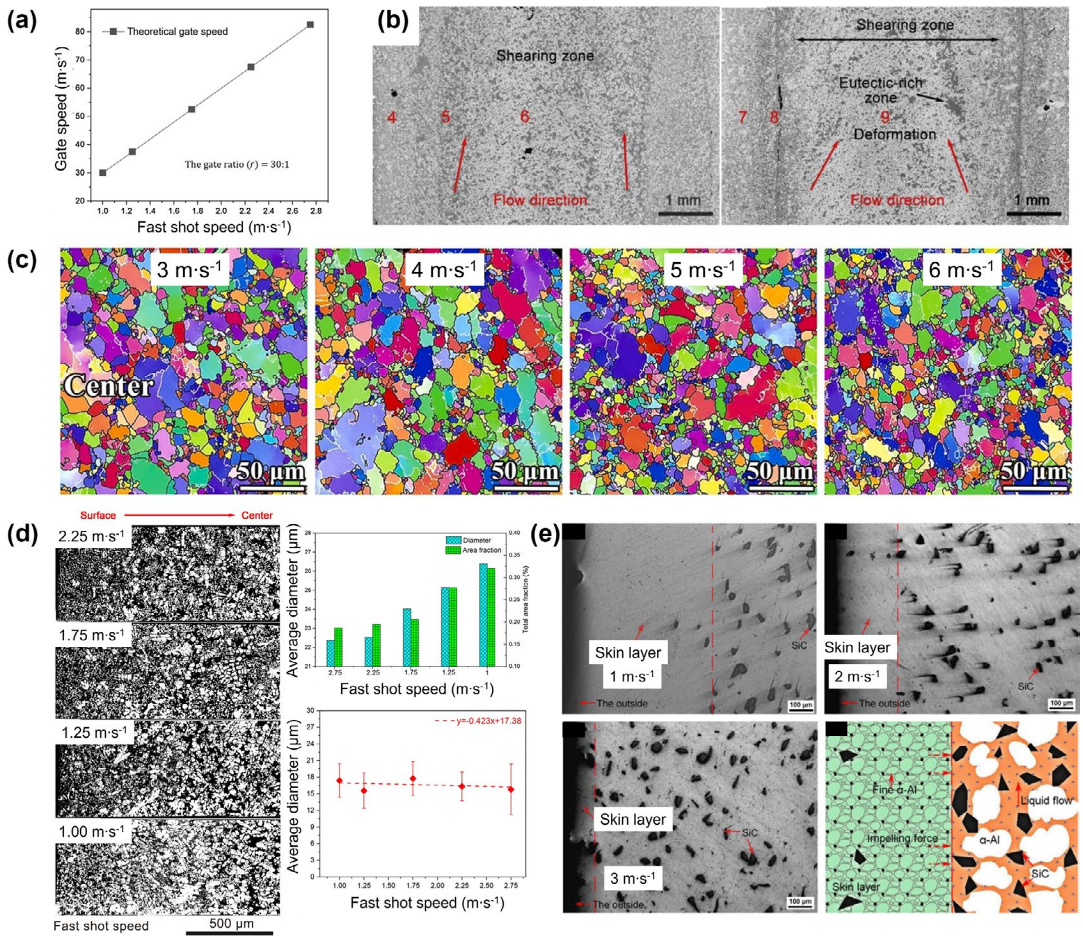

Fig. 2: Impact of fluid flow during fast shot phases: (a) relationship between fast shot speed and gate speed[41]; (b) optical micrographs of the shear zone[24]; (c) EBSD microstructures at different fast shot speeds[15]; (d) effect of fast shot speed on the morphological characteristics, equivalent diameter, area fraction, and secondary dendrite arm spacing of AlSi10MnMg alloy[41]; (e) outer microstructures of 6061-SiC composite samples under different fast shot speeds[46]

simulate the complex flow behavior within the shot sleeve by computing melt flow, heat transfer, and solidification[47]. Governing equations based on the enthalpy method[48] were applied, with melt turbulence characterized by the standard k-ϵ turbulence model[49]. The volume of fluid (VOF)[50] method was implemented to capture the dynamic evolution of the free surface. Results indicate that near-wall regions exhibit boundary layer development due to frictional forces between the molten metal and the shot sleeve and die surfaces. Additionally, impingement of the superheated melt onto the relatively cooler shot sleeve and die surfaces induces time-dependent variations in the interfacial heat transfer coefficient (HTC). This method can capture the transient thermal interactions at the metal-sleeve interface and predict the impact of slow shot speed on the subsequent solidification process.

Although increasing fast shot speed can enhance fluidity due to an increase in kinetic energy of the metal fluid, this increase is inherently constrained by the capacity of the HPDC machine, which imposes an upper limit. Additionally, higher shot speeds elevate the Reynolds number (Re), intensifying turbulence within the die cavity. As the plunger speed decreases, the effect of heat transfer on fluidity diminishes compared to the latent heat[51]. For a fixed-volume die, the shift from high Re to near-zero values during the casting process creates variations in microstructure along the flow path. Such changes lead to performance discrepancies across different regions of the component, which impact the service life of the die-cast part due to uneven material properties and degraded structural integrity.

2.1.3 Intensification pressure phase

The injection process in HPDC is divided into three primary phases: slow shot (Stage 1), fast shot (Stage 2), and intensification pressure (IP, Stage 3)[38]. The IP phase, which follows the fast shot phase, consists of both the applied pressure and holding time. The IP value for different purposes is about tens of MPa, which is one of the major factors governing the porosity level in the HPDC process. As shown in Fig. 3(a), an increase in IP prolongs the freezing time at the gate. This extended period allows for effective shrinkage compensation, which helps alleviate defects caused by rapid solidification, finally enhancing fluidity[52].

The influence of intensification pressure on solidification time is due to variations in the convection heat transfer coefficient (HTC) and heat flux at the gate induced by changes in pressure levels. However, increased pressure appears to have minimal impact[53] on the HTC compared to the gate speed and the die temperature [Fig. 3(b)]. Additionally, IP can

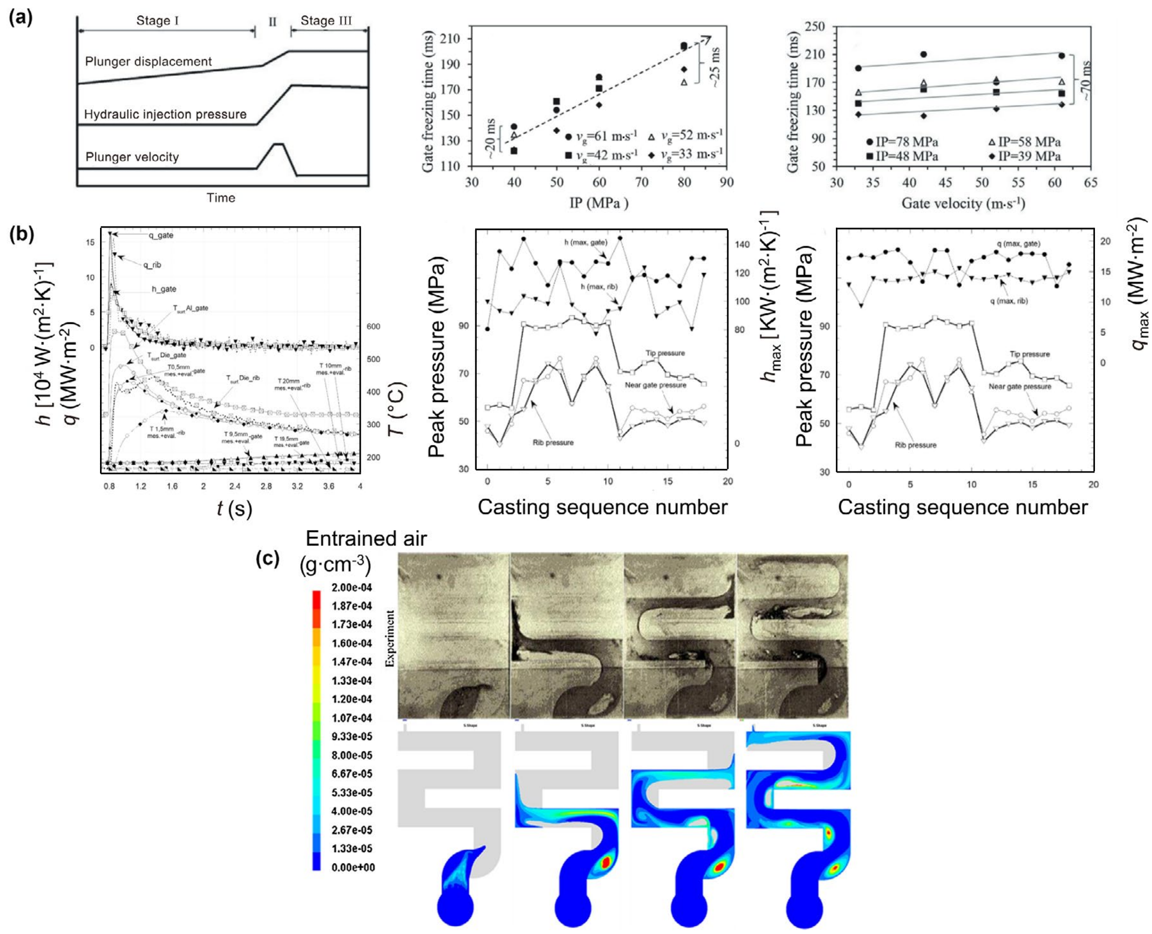

Fig. 3: Impact of IP phases on fluid flow: (a) schematic diagram of the IP phase and gate freezing time changing with IP and gate speed[38, 58]; (b) heat transfer results for the A380 alloy obtained using the inverse model approach, and the variation of maximum heat flux and HTC with respect to in-cavity pressure[53]; (c) simulation results of entrained air and flow behavior during IP phases[5, 59]

suppress pore diffusion and growth, thereby reducing defects caused by insufficient fluidity [Fig. 3(c)]. The increase in solidification time and fluidity may be due to higher pressure reducing backflow[54] around the location where flow direction changes. Reduced backflow also explains the decrease in air entrainment and pore formation.

It has been recognized that the purpose of IP is to compensate for shrinkage[55]. Therefore, the thermal expansion needs to be equal to the mechanical contraction due to the pressure, as described by volumetric Hooke's law. Lee et al.[56] found that porosity is reduced with increasing IP. The pressurization size, including gate areas and flow paths, directly impacts fluidity. Smaller gates or narrow runners restrict flow and increase pressure loss, potentially leading to early solidification and reduced casting quality. Conversely, larger runners can improve metal flow but may heighten turbulence. Overflow reservoirs enhance the quality of large runner castings by controlling excess metal and pressure, ensuring continuous flow, and minimizing turbulence. Additionally, the positioning of gates and inlets affects how evenly the molten metal fills the cavity. Poor gate placement can lead to uneven filling, air entrapment, and cold shuts.

Otarawanna et al.[57] suggest that elevated IP induces dilatant shear band in the gate region during the intensification stage, which appears to facilitate feeding during this stage. However, this process requires sufficient IP, which in turn demands a high locking force. When shear bands are present at the gate, the material is pushed through the gate and into the die cavity by localized deformation in a weaker shear zone. Therefore, shear band is part of the feeding mechanism during the intensification stage at high IPs. The absence of shear bands through the gate at low IPs suggests that the applied stress was insufficient to initiate shear band in the partially solidified gate material. Although not observed in this case, defect bands do exist in the runner, and multiple bands are occasionally observed within a single cross-section. Bands located closer to the center of the cross-section are more susceptible to contain porosity or large cracks due to feeding difficulties as they solidify later than those closer to the surface.

2.1.4 Gating ratio

The gating ratio (Ω), defined as the ratio of the cross-sectional area of the sprue (S_s) : total runner area (S_r) : total ingate area (S_g), characterizes the relative dimensions of the components in a gating system. This ratio, in conjunction with the fast shot speed, directly governs the initial velocity of the molten metal as it enters the die cavity through the ingates[60, 61], represented as:

$$\Omega = S_s : S_r : S_g \tag{3}$$

Increasing the gating ratio proportionally increases the velocity of the fluid in the gate. This system is called gate control system because ingates control the flow of the metal[62]. In HPDC process, the gating ratio can be simply described as the ratio of the plunger cross-sectional area to the gate cross-sectional area. The relationship between the gate speed and the fast shot speed can be described as:

$$v_{gate} = \frac{S_{plunger}}{S_{gate}} \cdot v_{fast} \tag{4}$$

where v_{gate} is the gate speed, v_{fast} is the fast shot speed, and $S_{plunger}$ and S_{gate} are the cross-sectional areas of the plunger and gate, respectively.

The gating ratio depends on the sizes of the plunger and gate in the die. It is influenced by process conditions and can be adjusted through design. It can be derived from the continuity equation[63] and momentum conservation. A higher gating ratio means the liquid in the runner moves faster at a given fast shot speed, improving the fluidity of the molten metal. However, continuously reducing the gate size to increase the gate ratio does not indefinitely improve fluidity. A smaller gate shortens the solidification time of molten metal in the runner, causing early solidification that obstructs subsequent flow. Eventually, the metal that does not reach the runner will thicken the biscuit and solidify in the shot sleeve. For Al alloy, gate speed has been analyzed as one of the significant variables affecting fluidity[20].

2.1.5 Die parameters

Die parameters include temperature, material, coating, and permeability. The die and melt temperatures determine the heat transfer, which affects molten metal fluidity[64]. Generally, fluidity increases with higher die temperatures, indicating a lower heat flux. In pure Al, this reduction may result from the rapid detachment of its chill layer from the die, decreasing thermal conductivity between the materials[65]. Rapid cooling under HPDC reduces fluidity by causing premature solidification, while higher die temperatures allowing a longer solidification time[52]. Under HPDC conditions, heat transfer involves both convective heat transfer and thermal conduction due to the combined effects of high flow speed and solidification. The heat flux is the function of the thermal conductivity of the fluid, the convective HTC between the fluid and the die, the thermal conductivity of the die, and the temperature difference between die and fluid. It can be written as:

$$q = -\lambda \frac{\mathrm{d}T}{\mathrm{d}x} = \frac{(T_m - T_f)}{\sum \frac{l_i}{\lambda_i} + \frac{1}{h_f}} \tag{5}$$

where q is the heat flux, λ is the thermal conductivity between the melt and the die wall. λ_i is the effective thermal conductivity between the melt and the die wall through the solidified shell after solidification begins, assuming that the shell consists of i layers, h_f is the convective HTC, l_i is the heat transfer medium length, and T_m and T_f are the temperature of die and molten melt, respectively[66].

Different die materials have varying thermal conductivities and heat capacities, which affect the cooling rate of the molten metal and its fluidity[67]. For instance, in HPDC, the most widely used die material is H13 steel[68-70]. Its thermal conductivity does not change much with temperature and is about 24.3 W·m^{-1}·K^{-1} at 500 °C.

The addition of specific metal oxides (such as aluminum silicate) and surface-active materials[67] in die can improve the fluidity of molten metal, enabling the production of castings with complex geometric shapes. Liu et al.[71] used a novel ceramic-type shot sleeve (LX sleeve) instead of the conventional H13 steel sleeve. This reduced the formation of ESCs, leading to improved mechanical properties and thermal conductivity. Furthermore, the LX sleeve produced smaller, less dendritic ESCs, reducing porosities, especially shrinkage porosities. This resulted in better elongation and thermal conductivity (120.6 $W\cdot m^{-1}\cdot K^{-1}$ vs. 112.2 $W\cdot m^{-1}\cdot K^{-1}$). Using these kinds of shot sleeve can also reduce the cooling rate in the shot sleeve, which could reduce the amount of heat lose by the fluid in the sleeve, and thus leads to an increase in the flow length.

Wettability is the ability of a liquid to spread on a solid surface[72]. Fluid flow rates are higher in systems with good wettability compared to systems with poor wettability. This is because systems with good wettability reduce the frictional resistance between the fluid and the die material, thereby enhancing fluid flow[18]. Wettability is primarily measured by the contact angle, with smaller contact angles indicating better wettability[73].

The roughness of the die surface also affects fluid flow[74]. Rough surfaces increase the frictional resistance between the fluid and the die. The texture of the die can also influence the fluidity. A smoother die surface reduces the resistance to flow. Conversely, rough surfaces can impede the flow of the metal, causing the formation of surface cracks during the pullout process[75]. Therefore, the die surface needs to be polished to reduce surface roughness. The permeability of a die refers to its ability to allow gases to escape from the die cavity[76]. With increasing permeability, the higher fluidity has been observed[77]. For the gas venting and pressure equalization, during the filling process, gases such as air or decomposition gases from the material being processed can become trapped within the die cavity. If the die has poor permeability, these gases cannot escape effectively, leading to pressure build-up that can hinder the flow of the material. In that case, low permeability can cause back pressure[18, 78] from the gases in the die. This pressure opposes the flow of molten metal, hindering its ability to fill intricate or thin sections of the die. Therefore, the proper design of exhaust positions and exhaust systems (vacuum systems) can reduce back pressure, finally improving fluidity.

2.1.6 Die shape

For flat plate type die, a component originally designed for crash testing of ductile materials was adapted to assess the fluidity of materials in ultra-large castings[2]. The die material is H13 tool steel with a hardness (Rockwell scale) of HRC 52 to 55. To meet engineering requirements, flat plates and nearly 90° ribs were incorporated. A casting measuring 635 mm×220 mm×2.8 mm achieved a maximum flow length of 1,230 mm in a 2.8 mm thick channel [Fig. 4(a)]. The runner system and overflows were optimized and integrated with cooling channels, heating channels, vacuum system, and spray controls.

By using this die, a new concept of effective flow length was introduced, combining both geometrical soundness and mechanical properties to evaluate castability. Features such as flat plates and sharp 90° ribs were designed to simulate integrated die casting conditions; however they introduce challenges, including turbulent flow and rapid solidification in narrow sections[79]. The rib structures increased the risk of defects like porosity and incomplete filling at lower temperatures and slower in-gate velocities. Mechanical properties varied significantly with the distance from the runner. While yield strength remained consistent, elongation decreased dramatically along the flow path due to porosity and uneven cooling. Consequently, in the HPDC process, die geometry and process conditions need be tailored to strike an optimal balance among fluidity, defect minimization, and the achievement of uniform mechanical properties.

The most commonly used die shape is the spiral shape. A spiral die was employed to evaluate fluidity, as illustrated in Fig. 4(b)[80]. The die featured a channel width of 7 mm, with wall thicknesses of 0.5 mm, 0.8 mm, and 1.0 mm. The total length of the die was approximately 700 mm. For the fluidity test, a crimp was positioned at the tip of the spiral test piece. The crimp and the unfilled section were excluded from the measured flow path[80]. This type of die can be used to study the effect of wall thickness on fluidity. Generally, for thin-walled castings, increasing the wall thickness improves fluidity[81]. This is because the higher volume increases the internal energy of flow, which delays the choking time.

Kim et al.[82] used a snake-shape die to measure the fluidity of Al alloy, wherein the length of the solidified casting sample was measured, served as a direct indicator of melt fluidity, as shown in Fig. 4(c). Additionally, an experimental die made of H13 steel was used for the study of fluidity under HPDC conditions. Figure 4(d) shows an Al casting made by using this die. A fluidity specimen, identical to a fluidity spiral, was produced in a thin fluid test channel measuring 1 mm thick, 15 mm wide, and 914 mm long. The die was designed for two purposes, one for measuring fluidity length and the other for measuring hot tearing (cracking) tendency[83]. The die shown in Fig. 4(e) is a dual-purpose die commonly used in HPDC, typically used alongside plate and rod specimens. Although it was not explicitly designed as a fluidity test geometry, it can qualitatively indicate melt fluidity under low-speed filling conditions[84]. Additionally, rods and plates can be directly used for mechanical properties testing.

The complexity of the geometry, die wall thickness, corner design, and transition areas between sections of differing thickness can influence fluidity. Consequently, these geometric features are critical variables in die design. In Fig. 4(b), different wall thicknesses in die design are discussed. Wall thickness plays a crucial role in determining whether the one-dimensional heat transfer condition is met and significantly influences the solidification behavior of alloys. Regarding the complexity of die geometry, current mainstream approaches to measuring fluidity under HPDC conditions typically focus on designing sufficiently long flow paths within a limited volume. Figures 4(b)–(d) show a ring-shaped channel design.

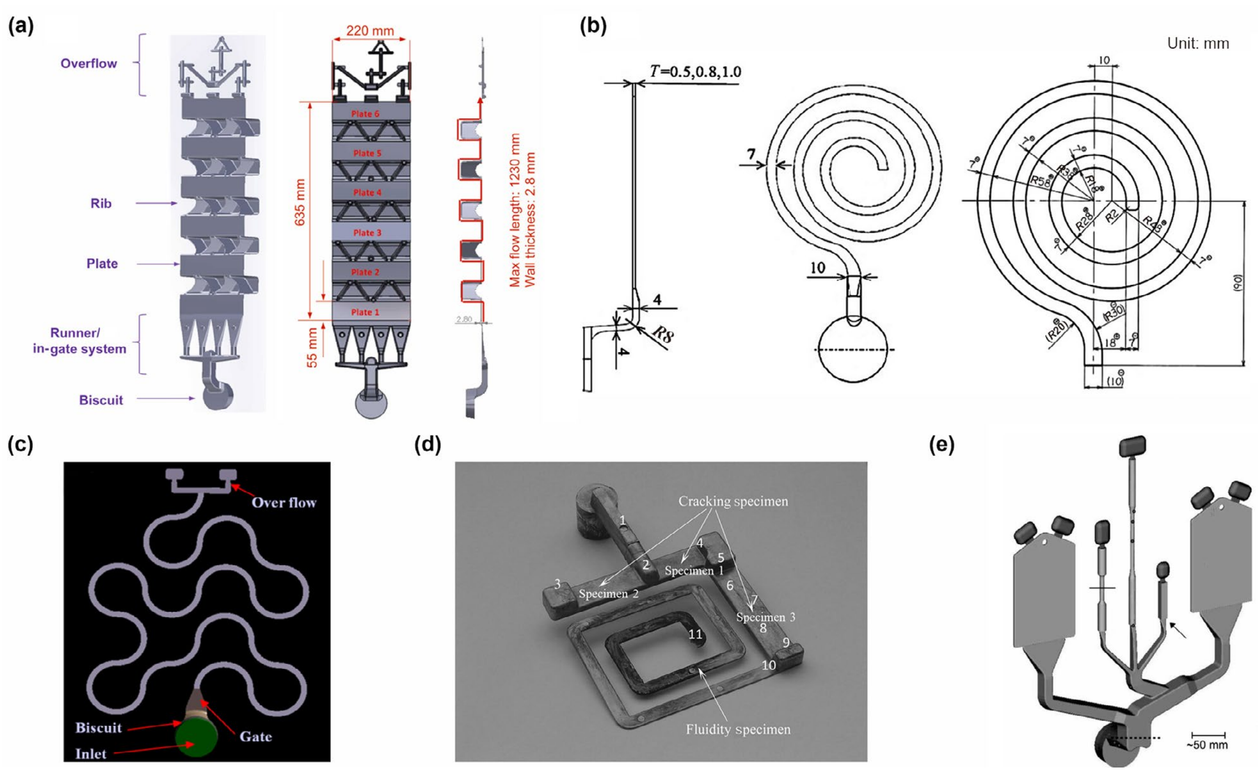

Fig. 4: Different shaped dies for measuring fluidity: (a) flat plate die[2]; (b) spiral die[80]; (c) snake shape die[82]; (d) hot tearing tendency and fluidity dual purpose die[83]; (e) mechanical properties and fluidity dual purpose die[84]

This design is simple and meets the experimental requirement of measuring alloy fluidity using low-tonnage die casting machines. The design of corners and transition areas in the die is critical. As shown in Fig. 4(d), the die features a variable cross-section at the corner intended for evaluating hot cracking tendency. However, this design makes it difficult to distinguish between cracks caused by hot tearing and those caused by insufficient fluidity. Moreover, as noted in the statement in Section 3.2, such variable cross-sections tend to cause flow choking. Therefore, it is preferable to design dedicated dies for fluidity measurement, avoiding variable corners, cross-sections, and complex transitions in the main channel.

According to the reviewed literature, there is no unified standards for die shapes used for fluidity measurement, creating challenges for experiment repeatability and fluidity comparisons across different die designs. Developing a universal fluidity test standard is a potential solution to this issue.

2.2 Metallurgical variables

Considering the complex effects of metallurgical variables on fluidity, particularly with respect to composition, remains a significant challenge. Experimental characterization and simulation have demonstrated that alloys with eutectic composition exhibit solidification behavior akin to that of pure metals[85], achieving elevated fluidity. However, findings indicate that the composition yielding optimal fluidity in some Al-X alloys (X represents other elements) deviates from the eutectic point. Consequently, composition alone cannot serve as a definitive criterion for evaluating fluidity. A comprehensive assessment should incorporate other metallurgical variables, including superheat, latent heat, surface tension, viscosity, and solidification mode .

Controlling fluidity through metallurgical variables has several technologies beyond HPDC, extending to welding, additive manufacturing, continuous casting, and injection molding. Composition design and other related factors impact the structure-fluidity relationship, with metallurgical variables proved as influential casting variables. The next discussion will explore how specific variables affect fluidity and the complex interdependencies among them, highlighting the mechanisms and phenomena that shape fluidity outcomes.

2.2.1 Composition

Alloying elements impact the fluidity of Al alloys under HPDC conditions by altering properties such as viscosity, latent heat, surface tension, and solidification interval. Elements like Si can shift the solidification mode from skin forming to equiaxed growth[86], consequently decreasing fluidity[87]. However, increasing Si content or other alloying elements does not universally reduce fluidity. Figure 5(a) illustrates the fluidity variation of binary Al-Si, Al-Mg, and Al-Cu alloys with element content. The fluidity increases initially, peaks before the eutectic composition, and then decreases. Notably, the fluidity does not reach its maximum at the eutectic point but peaks at the hypereutectic composition before decreasing.

Al-Si alloys are employed in large-scale casting production, attributed to their superior fluidity[10]. For Al-Si alloys, fluidity is sensitive to compositional factors[88, 89]. Elements such as Fe, Mn, Mg, Zn, Ti, Zr, etc.[90–92] added to aluminum alloys will affect the fluidity of the alloy on varying degrees and different trends.

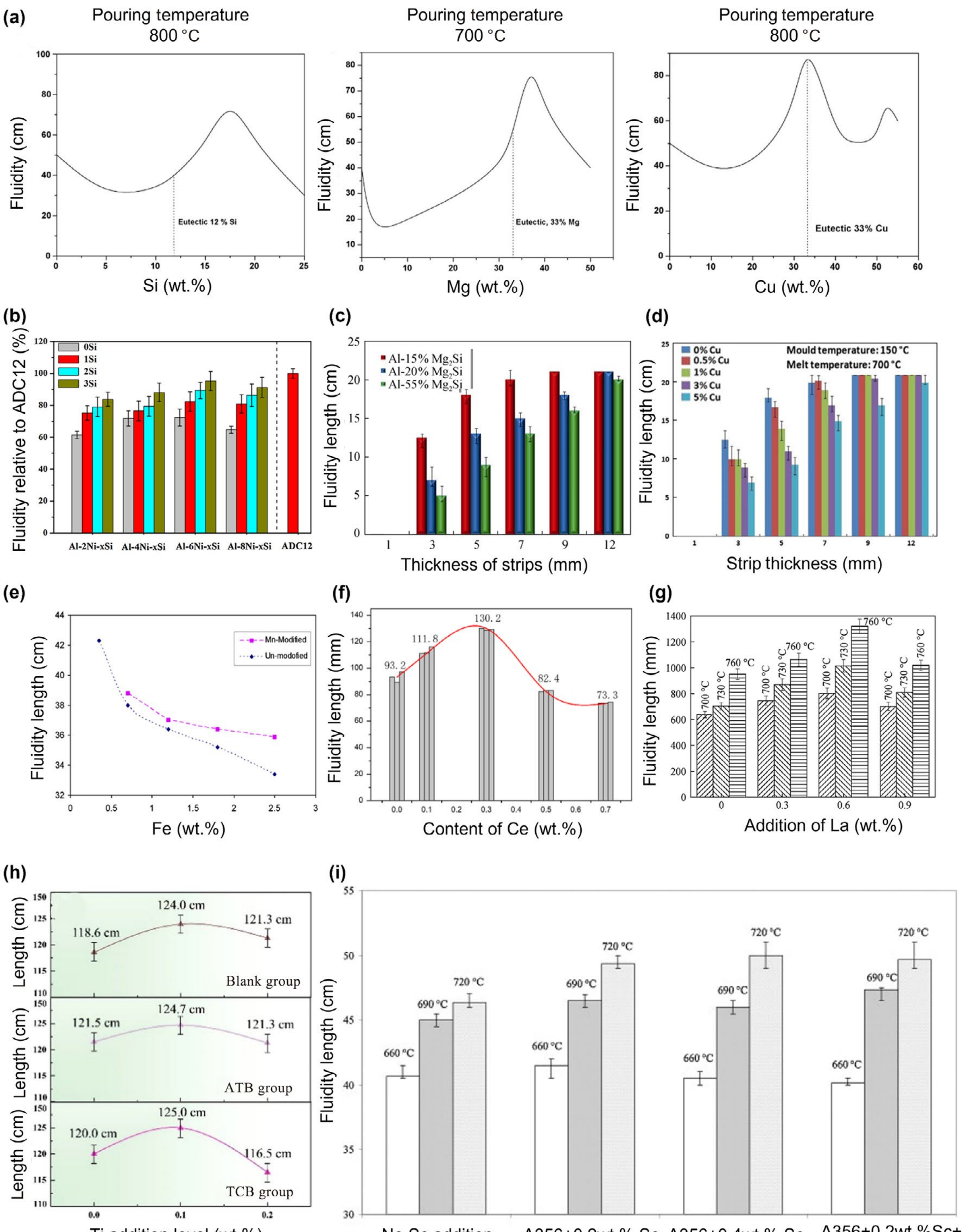

Fig. 5: Effect of different element additions on the fluidity of Al alloys: (a) effect of element addition on fluidity of binary Al-Si, Al-Mg, Al-Cu alloys[119]; (b) effect of Si content variation in Al-Ni-Si alloy on fluidity[120]; (c) fluidity variation trend of Al-Mg_2Si composites with different Mg_2Si content[98]; (d) fluidity variation trend of Al-Mg-Si alloy with different copper content[100]; (e) effect of Fe content on fluidity in 413 alloy[103]; (f) effect of Ce content on fluidity in A356 alloy[121]; (g) effect of La content on fluidity in ADC12 alloy[122]; (h) effect of Ti content on fluidity in Al-7Si alloy[123]; (i) effect of Sc and Zr content on fluidity in A356 alloy[113]

Alloys exhibit higher fluidity when solidification proceeds via a planar front mode, indicating that specific solidification behaviors strongly influence casting performance. Research found high latent heat of Si released during primary Si formation[93]. Non-dendritic primary Si particles create a more fluid melt, unlike Al dendrites that impinge and cohere. Ragone et al.[94] indicate that fluidity is influenced by the solidification interval. Specifically, a narrower solidification range results in better fluidity. For the Al-Ni-Si ternary alloy system, with a fixed Ni content, the fluidity increases gradually as the Si mass fraction rises from 0% to 3%, showing a trend different from binary alloys [Fig. 5(b)]. When the Si content is fixed, the fluidity increases initially and then decreases as Ni content increases from 2% to 8%. However, it has been verified that the highest fluidity occurs at Al-2Si-0.5Ni, attributed to the ternary eutectic reaction of Al-Al3Ni-Si[95]. Additionally, increasing Ni content beyond 1wt.% reduces fluidity due to the formation of coarse, blocky Al_3Ni intermetallics.

Magnesium is added to Al-Si alloys to improve strength[96, 97]. However, the presence of Mg reduces fluidity due to the formation of Mg_2Si phases, which expand the solidification range and increase melt viscosity[98, 99]. Figure 5(c) shows that the fluidity of the melt decreases significantly as the magnesium (Mg_2Si) content increases.

In Al-Si-Cu alloys, copper is added to increase strength, but it reduces fluidity by broadening the solidification interval[100], which promotes premature solidification. Figure 5(d) shows a significant decrease in the fluidity of the Al-Mg-Si alloy as the Cu mass fraction increases from 0% to 5%. In Al-Cu alloys, fluidity initially decreases with Cu additions (≤10wt.%) but improves as the alloy approaches eutectic compositions. Furthermore, the Cu enrichment escalates the hot tearing sensitivity and diminishes fluidity[101], predominantly due to an expanded solidification range and an increased propensity for dendritization.

Iron (Fe) is generally considered harmful to the mechanical properties[102] and fluidity[103] of HPDC alloys. However, less than 0.20wt.% Fe is added during melting to aid demolding after solidification of Al-Si alloys. It has been reported that the Fe-containing intermetallic phases can be modified by adding Mn, transforming the β Fe-rich phase into the α Fe-rich phase and altering its morphology from needle-like to block-like[104]. Figure 5(e) shows that increasing Fe content gradually reduces fluidity. However, the test results with Mn modification indicate that the decline in fluidity is mitigated but still present.

In recent years, the addition of rare earth elements (RE) such as Ce and La has been shown to enhance the mechanical properties[105] of Al alloys, with studies indicating that Ce specifically improves heat resistance[106]. The effects of these two REs on fluidity are similar, both initially increasing fluidity before causing a decline. For A356 alloy, fluidity peaks with the addition of 0.3wt.% Ce [Fig. 5(f)], while for ADC12 alloy, it peaks with 0.6wt.% La [Fig. 5(g)]. The addition of RE leads to the formation of nanoscale phases during the rapid solidification of HPDC. Ce enhances the nucleation of α-Al grains due to constitutional supercooling and the small lattice mismatch between $Al_{11}Ce_3$ and α-Al. Furthermore, the exothermic peaks were introduced in the solidification curves, occurring between the precipitation of the primary α-Al phase and the Al-Si eutectic reaction[107]. These effects may explain the initial increase in fluidity. However, as the content increases further, the precipitation of coarse second phases may reduce fluidity.

Figure 5(h) illustrates the fluidity of AlSi7 alloy with increasing Ti content. The fluidity peaks at 0.1wt.% Ti. Ti is primarily added to HPDC Al alloys as a grain refiner, enhancing grain refinement and strengthening. While in higher concentrations, fluidity was reduced because the grains can block the advancing melt. Additionally, a vacuum fluidity test on Al-4.5% Cu alloy with 0.15% Ti addition showed a reduction in fluidity[108]. In A356 alloy with $AlTi_5B_1$, addition the fluidity decreased below 0.12% Ti but increased above this level by using sand spirals dies[109]. Kwon et al.[108] observed an increase in fluidity in A356 alloy containing 0.03wt.% Ti, with addition of $AlTi_5B_1$. It has been shown that the addition of Ti has varying effects on fluidity depending on the alloy composition.

Adding Sc to Al alloys enhances strength, corrosion resistance[110], and reduces hot tearing tendency[111], while the combined addition of Sc and Zr provides effective grain refinement[112]. For fluidity, Fig. 5(i) shows that Sc addition causes fluidity to fluctuate, initially increasing and then decreasing. With the addition of Zr, the fluidity decreases slightly. This phenomenon is generally consistent with the effect of Ti addition. The influence of Sc on fluidity is closely related to the presence of other elements. Although 0.4wt.% Sc resulted in the finest grain size, it did not further increase fluidity compared to 0.2wt.% Sc or 0.2wt.% Sc+0.2wt.% Zr samples[113]. Additionally, Sc modifies the eutectic Si structure, making it finer and more fibrous, which correlates positively with fluidity. In some cases, grain refinement can increase fluidity by postponing the dendrite coherency point (DCP). However, grain refinement can also decrease fluidity by increasing the number of solid particles in the melt.

Ca and Sr are commonly used as modifying elements in Al-Si alloys to refine Si structures, which enhance strength and elongation. Colak et al.[114] found the increase in the fluidity was established with Sr modification in Al-Si alloy. The effect of Ca addition on the fluidity of Al alloys has not been reported in the reviewed literature. However, it has been reported that Ca improves fluidity due to its refinement effect in Mg alloy. While excessive Ca content can lead to the formation of an oxide film on the melt surface, which have negatively impacts on fluidity[115, 116].

Finer grain structures generally improve fluidity with minor additions, as smaller grains reduce flow resistance. The DCP[117] is the temperature at which dendrites begin to overlap and form a network. Alloys with a greater difference between the pouring temperature and DCP provide more flow time. Alloying elements also influence the DCP, and delays in coherency trend to enhance fluidity by allowing a longer time for mass feeding. Besides, during the modification of Al-Si alloys, coarse Si particles are converted into fibrous particles[118]. Since fluidity is determined by the changes occurring at the initial stage of solidification, the effect of eutectic modifying agents in Al-Si alloys is expected to have a limited impact unless the Si content is close to the eutectic composition.

2.2.2 Superheat

Superheat refers to the temperature of molten metal above its liquidus temperature. Increasing superheat reduces the viscosity of the molten metal and increases the total energy of the system, which enhances fluidity and prolongs solidification time, though the relationship is not linear[124]. For the AlSi10MnMg alloy, an increase in superheat of 1 K results in an approximate 4.4%[125] increase in flow length over the temperature range of 923 K to 1,013 K [Fig. 6(a)].

Fluidity increases with superheat for a given alloy composition. Kolsgaard et al.[126] observed a linear increase in the fluidity of spiral sand castings with rising superheat. Specifically, an increase of 1 °C in melt temperature resulted in 1% increase in fluidity length within the temperature range of 700–760 °C. Similarly, Sahoo et al.[127] measured the fluidity of an Al-8.3%Fe-0.8%V-0.9%Si alloy using a standard spiral sand die. They reported an increase of 0.4% in fluidity for every 1 °C rise in melt temperature within the range of 860–900 °C. These fluidity results are not measured under HPDC conditions but qualitatively reflect the influence of superheat on fluidity.

The effect of increasing superheat on fluidity is not only due to the increase in system energy but also due to changes in grain size[128]. As shown in Fig. 6(b), the size of primary aluminum grains (α_1-Al) decreases with increasing superheat, while the size of secondary aluminum grains (α_2-Al) increases slightly. This fine-grain strengthening enhances both ultimate tensile strength (UTS) and elongation. However, Al MMCs (Al alloy-*x*vol.% SiC composites) exhibit different behaviors. Increasing melt superheat has negative impacts on the fluidity of Al MMCs. At higher temperatures, a chemical reaction occurs between SiC and Al, forming Al_4C_3, which leads to a decrease in fluidity[129].

Figure 6(c) shows the simulation results of filling at different superheat levels. At a superheat of 10 °C, the metal flows freely but forms fragmented bands with significant spray and moderate wall accumulation. At 0 °C (liquidus temperature), the flow remains similar, with spray, fragmentation, and mild connections to the runner. At –10 °C, fragmentation decreases, the main deposits become contiguous with the gate and runner. At –15 °C, the flow changes significantly, with minimal spray, smooth deposits, and a well-defined metal surface. At –20 °C, the flow becomes smooth, with no spray or jetting, resembling thixoforming rather than HPDC due to increased solidification and viscosity.

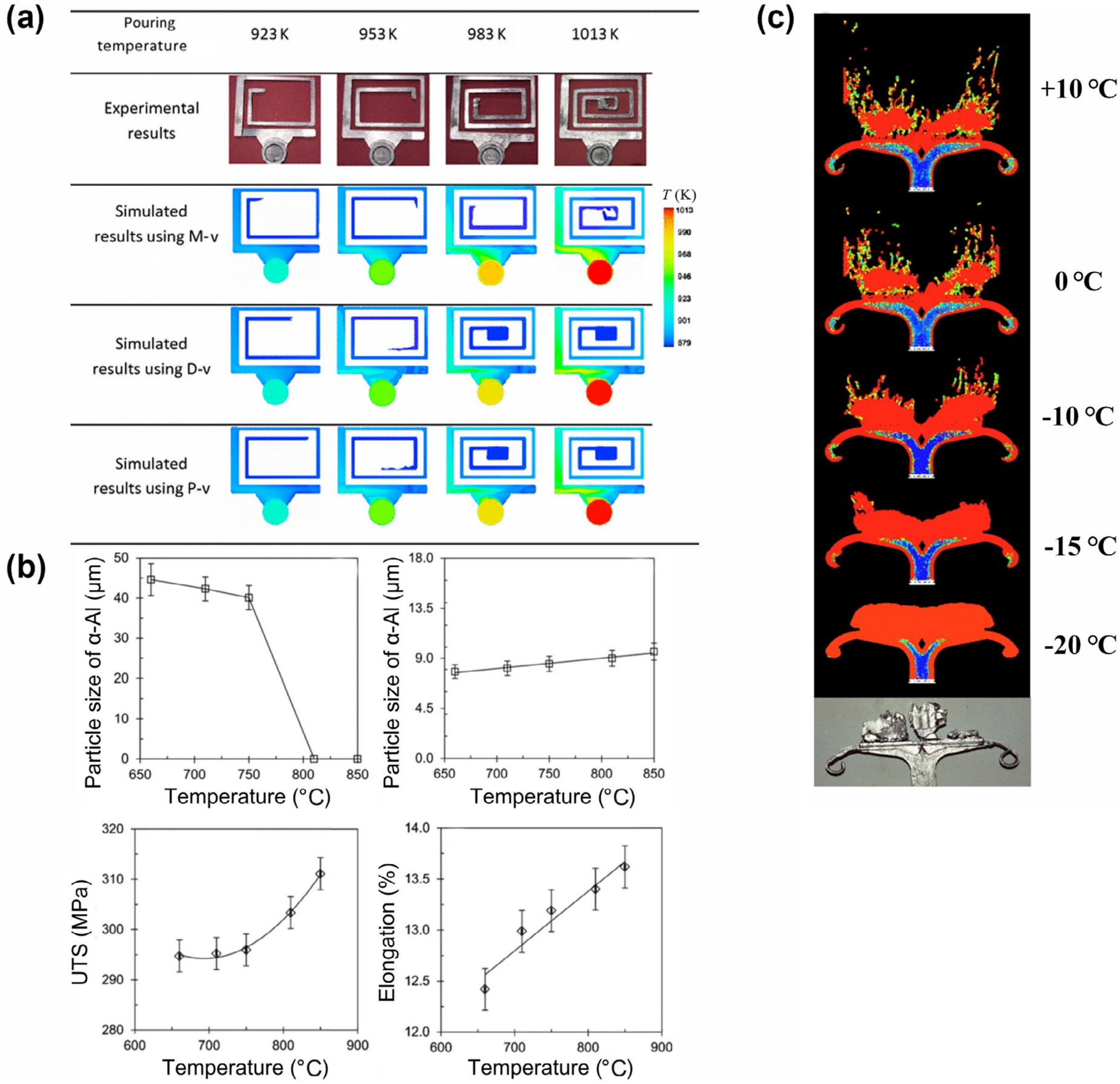

Fig. 6: Explanation of superheat in HPDC technology and its influence on fluidity and grain size: (a) comparison of experimental results with different simulation methods[125]; (b) effect of superheat on grain size of α_1-Al and α_2-Al, UTS, and elongation[128]; (c) short shot variation for a 10% fill with different superheat and actual product[124]

2.2.3 Latent heat

Latent heat refers to the energy released or absorbed by a material or thermodynamic system during a constant temperature process, typically associated with a first-order phase transition[130]. It is notable that Si has the relatively high specific latent heat of fusion compared to metallic elements (1,650 to 1,800 kJ·kg^{-1})[131]. Figure 7(a) lists the relationship between the (volumetric) heat of fusion and the melting point of some metal elements. The melting point and the latent heat of fusion need to be experimentally obtained[132] using calorimetric methods as differential scanning calorimetry (DSC) or differential thermal analysis (DTA).

Figure 7(b) shows a DSC result of AlSi7Cu1 alloy, the area of the peak is proportional to the latent heat. Additionally, the latent heat of fusion can be predicted for an *n*-component alloy using Eq. (6): the first part of the equation is the contribution of latent heat of pure elements; and the second part is the contribution of specific heat.

$$H_f = \sum_{i=1}^{n} x_i (H_f)_i \left(\frac{T_m}{T_i}\right) + T_m \sum_{i=1}^{n} x_i \left(c_{p,i}^{l} - c_{p,i}^{s}\right) \ln\left(\frac{T_m}{T_i}\right) \quad (6)$$

where x_i is the mole fraction, H_f is the latent heat of fusion, T_m is the melting temperature of the alloy, T_i is the melting temperature of the element, and c_p is the specific heat[133].

Despite DSC and DTA, the cooling curve and its derivative curve obtained using the calculation software[132] can also be used to simulate the value of latent heat and calculate its effect on fluidity [Fig. 7(c)]. Thermodynamic software tools like JMatPro, FactSage, and Thermo-Calc are used to predict the latent heat of alloys by relying on thermodynamic databases and models. These tools calculate latent heat based on Gibbs energy functions[134] for both liquid and solid phases as a function of temperature and composition. Using optimized thermodynamic parameters, the latent heat is derived as the difference between the enthalpy of the liquid and solid phases during solidification. The Scheil-Gulliver model[135], commonly used in these programs, assumes negligible solute diffusion in the solid phase and complete diffusion in the liquid phase, making it particularly effective for non-equilibrium solidification scenarios in alloys. Although these software tools are highly accurate for standard alloy systems with well-established databases, their precision depends on the quality and completeness of the underlying thermodynamic data.

Binary and ternary eutectic alloys of Al, Cu, Mg, Si, and Zn demonstrate the highest latent heat values[93]. Additionally, Lao et al.[136] reported a reduction in the latent heat of Al-Si alloys due to the gradual oxidation of Al. The latent heat of an alloy affects the fluidity by influencing the cooling rate and the temperature gradient during solidification. Higher latent heat can delay the solidification process, increasing the fluidity of the molten metal. For instance, the reason that Al-Si alloy exhibiting better fluidity than other Al alloy is that Si has higher latent heat than other elements.

2.2.4 Surface tension

Surface tension is an equilibrium thermodynamic property that plays a role in metallurgical processes comparable to that of viscosity. Surface tension is influenced by intermolecular potential energy and the liquid interfacial microstructure[137]. In contrast to viscosity, surface tension decreases with temperature and shows a nearly constant temperature dependence across

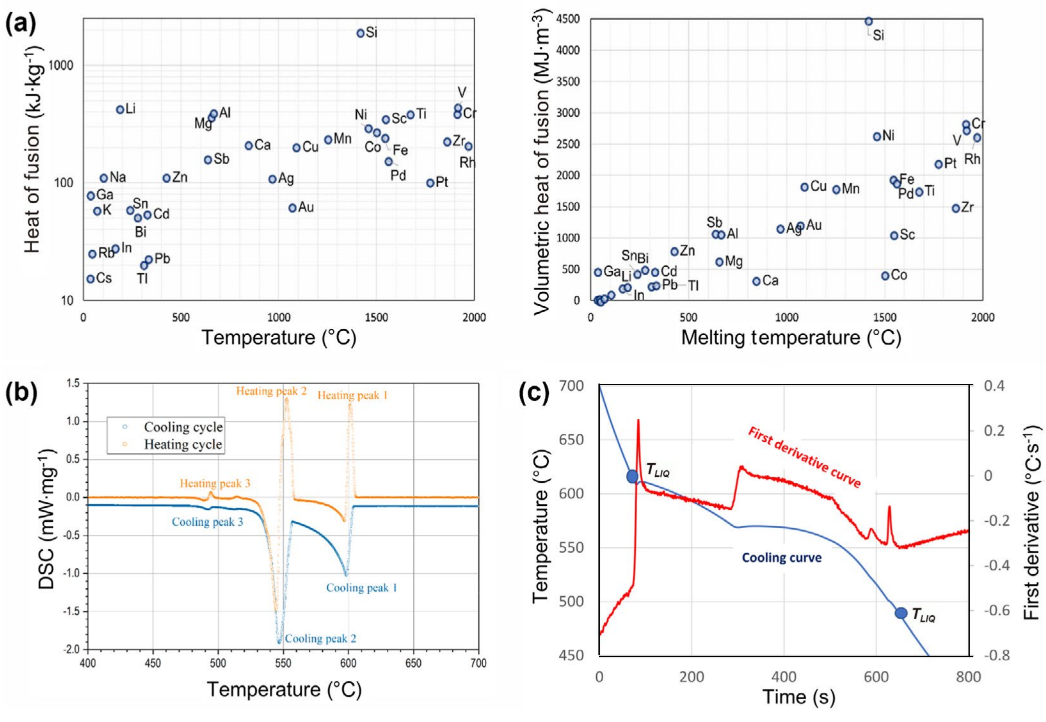

Fig. 7: Latent heat values of some elements and methods of measuring latent heat: (a) heat of fusion (latent heat) of some common metals and metalloids[93]; (b) DSC curves for cooling rate of 6 °C·min^{-1} for AlSi7Cu1 alloy[132]; (c) cooling curves and its first derivative for AlSi7Cu1 alloy[142]

most normal liquids[138, 139].

In the HPDC process, metals typically do not wet dies which will result in backpressure that resists the flow within the die. Die coatings and release agents are specifically designed to reduce backpressure. Consequently, the curvature of the meniscus at the melt front generates capillary repulsion. This surface tension-induced backpressure becomes more significant as the channel size decreases, counteracting the metallostatic pressure that drives the metal to fill the channel[140]. The net effective pressure (P_{net}) can be expressed as:

$$P_{\text{net}} = \rho g h - P_{\text{st}} = \rho g h - \gamma\left(\frac{1}{R}+\frac{1}{r}\right) \quad (7)$$

where ρ is the density, P_{st} is the back pressure due to the surface tension, γ is the surface tension, R and r are the two orthogonal radii that define the local shape of the surface; h represents the vertical height difference between the melt front during filling and the melt level in the shot sleeve. In gravity casting, the driving pressure is expressed as ρgh, which corresponds to the metallostatic pressure. In HPDC, ρgh can be interpreted as the driving pressure exerted by the plunger on the melt during the fast shot stage.

Several minor alloying elements, such as Li, Bi, Pb, Mg, Sb, Ca, and Sn, have been reported to reduce the surface tension of molten Al[16]. In contrast, the presence of surface oxides increases surface tension, acting as barriers to flow and negatively impacting fluidity[141].

2.2.5 Viscosity

Molten metal generally behaves as a non-Newtonian fluid, where the viscosity is not constant and depends on the frequency of shear applied to them. In physics, viscosity is considered the inverse of fluidity, however, viscosity is one of the factors that affect fluidity in HPDC. In Al alloys, viscosity, which measures flow resistance at a given shear rate, is affected by composition, temperature, and solidification behavior. For molten metals, viscous stresses depend on the shear rate rather than the extent of deformation. The Arrhenius model[143] is the most widely used empirical equation for calculating viscosity.

$$\eta = \eta_0 \cdot \exp(E/RT) \quad (8)$$

where η is the viscosity, η_0 is the pre-exponential constant, E is the activation energy for viscous flow, R is the gas constant, and T is the temperature.

For semi-solid HPDC process, the power law model is not only simple mathematically but also in good agreement with the experimental data, the equation is defined by:

$$\begin{cases} \eta_\alpha = k\dot{\gamma}^{n\text{-}1} \\ \bar{\dot{\gamma}} = \dfrac{1}{2} R_0 H_0^2 v_0 \left(H_0 - v_0 t\right)^{\frac{1}{2}} \\ \bar{\dot{\gamma}}_{\text{pipe}} = \dfrac{(12n+4)v_0}{(2n+1)(D_1 - 6\cot\alpha v_0 t)} \end{cases} \quad (9)$$

where η_α is the apparent viscosity, k is the consistency factor, $\dot{\gamma}$ is the shear rate, and (n–1) is the flow exponent (n=1 for Newtonian fluids). R_0 and H_0 represent the initial radius and height of the sample, respectively, v_0 is the velocity before the cross-section changes, t is the shear time, r is the radial distance from the centerline of the pipeline, D_1 is the instantaneous diameter of the pipeline, and α is the angle of the variable cross-section connection[144].

The viscosity of Al alloys decreases with increasing temperature [Fig. 8(a)], initially decreases and then increases with rising Si content [Fig. 8(b)], and decreases with increasing shear rate [Fig. 8(c)]. Through a recent review of viscosity, it has been reported that computer coupling of phase diagrams and thermochemistry (CALPHAD) approach and the ML method should be an effective strategy for predicting accurate viscosities in target alloy melts[145].

2.2.6 Solidification mode

It has been reported that the critical solid fraction at which flow stops is approximately 0.15 to 0.25 in gravity and sand casting conditions, while under HPDC conditions, a solid fraction of 0.5 is typical for solidification[148]. The maximum solid fraction at which flow stops depends on factors such as ram pressure, flow channel thickness, and grain size of the solidifying phases. With experimental statistics, the results

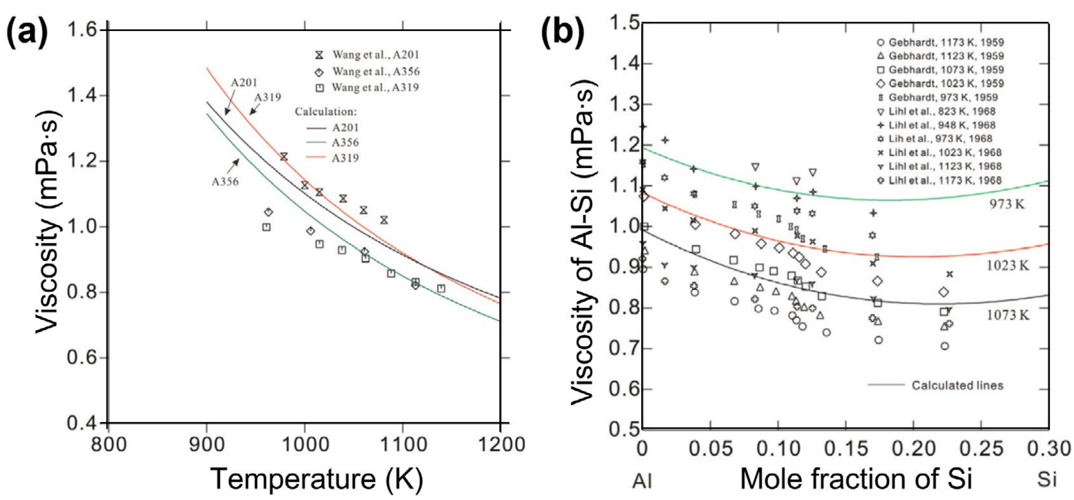

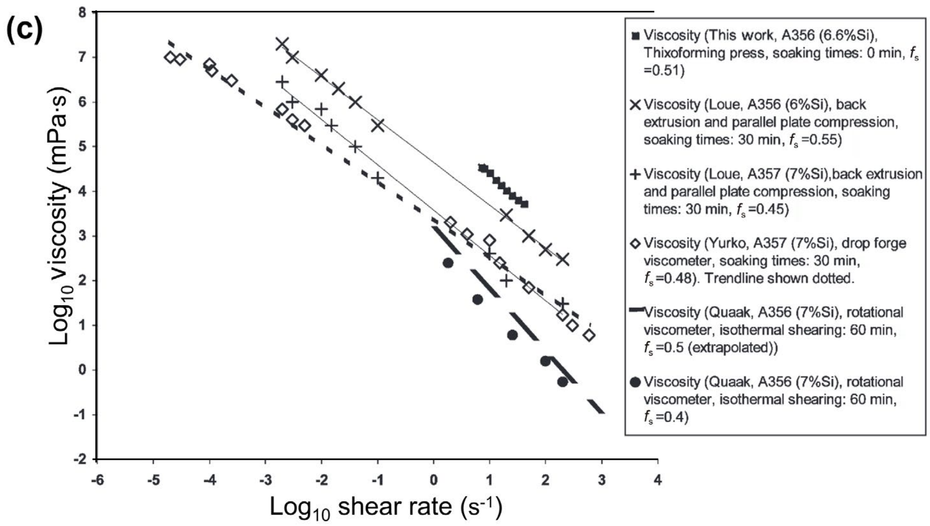

Fig. 8: Variation in Al alloy viscosity with different variables: (a) viscosity of the Al-Si system in different temperatures[146]; (b) calculated viscosities of selected Al alloys compared with experimental data[146]; (c) viscosity-shear rate curves[147]

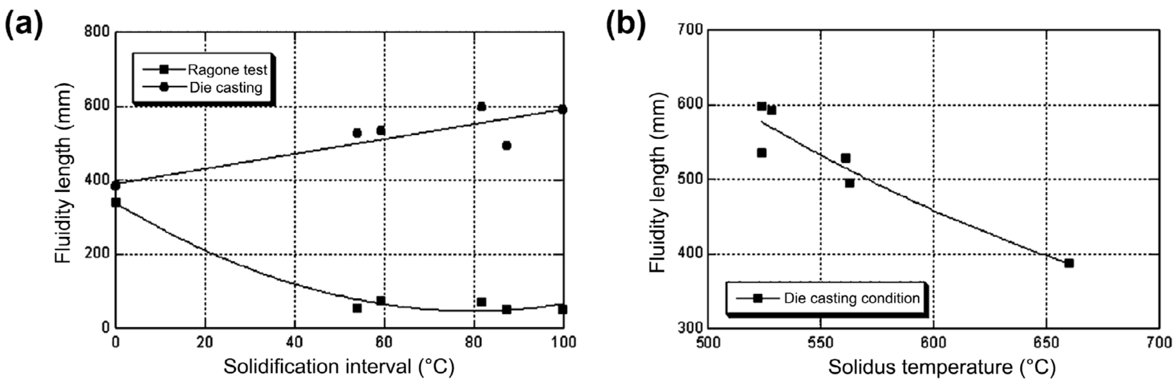

Fig. 9: Effect of phase diagram parameters on fluidity due to changes in the solidification mode: (a) relationship between fluidity and solidification interval in Ragone test and HPDC; (b) relationship between fluidity and solidus temperature in HPDC[83]

indicated that a smaller solidification interval improves fluidity in gravity casting [Fig. 9(a)], whereas a lower solidus temperature enhances fluidity in HPDC [Fig. 9(b)].

Under HPDC conditions, fluidity improves because the high flow rate increases the critical solid fraction at which the metal solidifies. Han et al.[83] suggest that flow stops when the solid fraction reaches approximately 0.6. Consequently, the temperature at which the flow front stops is closer to the solidus temperature, allowing most of the latent heat to be utilized for die filling. This explains the flow length increases as the solidus temperature decreases at a given superheat.

2.3 Flow variables (Indirect variables)

The die casting process primarily involves forced convection heat transfer, characterized by the evolution of temperature, velocity, and microstructure fields. However, natural convection should also be considered, as gravity inherently induces a certain degree of natural convection. Flow variables (indirect variables) are quantitative expressions reflecting the combined effects of casting and metallurgical variables. They primarily include dimensionless numbers related to forced convection heat transfer and natural convection heat transfer. The following sections will detail their basic concepts and impact on fluidity.

2.3.1 Dimensionless number

In fluid mechanics and heat transfer, numerous dimensionless numbers are defined to characterize various fluid flow scenarios and assist in model development. The definitions of these dimensionless numbers, along with their values in Al alloys in the HPDC process, are as follows:

$$\begin{cases} Re = \dfrac{\rho v L}{\mu}, \quad Re \in (0, 300000) \\ Pr = \dfrac{\nu}{\alpha}, \quad Pr \approx 0.019 \\ Nu = \dfrac{hL}{k}, \quad Nu \in (0.1, 1.0) \\ Ste = \dfrac{c_p(T_i - T_f)}{L_f}, \quad Ste \in (1.0, 4.0) \\ Pe = \dfrac{Lv}{\alpha} = Pr \times Re, \quad Pe \geq 100 \end{cases} \tag{10}$$

where ρ represents the density, v represents the flow velocity, L represents the characteristic length, μ represents the dynamic viscosity of the fluid, ν is the kinematic viscosity. α is the thermal diffusivity, h is the interfacial HTC, k is the thermal conductivity of the material, c_p is the specific heat, T_i is the initial temperature, T_f is the final temperature, L_f is the latent heat[51].

In order to identify the L, the hydraulic diameter was used to construct an applicable approximation:

$$L = \frac{4A}{P} = \frac{2d \cdot w}{d + w} \tag{11}$$

where A is the flow cross sectional area, P is the wetted perimeter of flow, d is the height of the channel, and w is the width of the channel.

Re[149] represents the ratio of inertial forces to viscous forces in a fluid. In HPDC, the high velocity flow enhances the role of kinetic energy in fluidity, overshadowing the effects of heat dissipation. A higher *Re* in HPDC compared to gravity casting indicates that inertial forces dominate the flow, enabling the metal to flow further even as solidification begins[150]. The target solid fraction also interacts significantly with the die temperature and injection speed, implying that alloys capable of flowing at higher fractions solid exhibit improved fluidity. Additionally, *Re* is closely related to turbulent flow in cooling channels. It is often used to determine the minimum flow rate required to maintain efficient cooling. In HPDC, the *Re* of the metal fluid typically decreases from hundreds of thousands to zero within hundreds of milliseconds[151], indicating a rapid transition from turbulent to laminar flow. Overall, the transition is influenced by a combination of material properties and process conditions.

Prandtl number (*Pr*) is defined as the ratio of momentum diffusivity to thermal diffusivity[152]. For $Pr<<1$, the length to fully developed velocity profile is much longer than the fully developed thermal profile[153]. For many metals with the *Pr* number is much less than 1, indicating that the velocity profile remains relatively flat and uniform upon entering a thin section, in contrast to the fully developed parabolic profile. For Al alloys, the *Pr* number (≈0.019) reveals that the temperature profile becomes fully developed much earlier than the velocity profile[51]. This suggests the velocity profile remains relatively flat and less parabolic.

Blass et al.[154] investigates the effects of the *Pr* on turbulent sheared thermal convection. Under the constant rayleigh number (*Ra*) (*Ra*=106), the *Pr* is changed from 0.22 to 4.6 (Fig. 10). Low *Pr* (e.g., $Pr\leq0.22$) weakens shear influence, which delays the onset of shear-dominated dynamics and mitigates the fluctuations of Nusselt number (*Nu*). The *Nu* is the ratio of total heat transfer to conductive heat transfer at a fluid boundary[155]. For $Nu<<1$, the material exhibits smaller temperature gradients throughout the casting, resulting in fewer thermal contours. In many of the common cast materials and thicknesses, the *Nu* is around 1. The *Nu* number in the range of 0.1 to 1.0 suggests that the interfacial heat transfer is at least as important for the heat transfer as the heat conduction in casting wall thickness.

Stefan number (*Ste*) is the ratio of the sensible heat to the latent heat in the material[156]. For $Ste>>1$, the sensible heat required to cool the material from the initial temperature to the final temperature is large compared to the latent heat. Metals cooling from liquid to die temperature can have a *Ste* number around 1 to 4. At a higher die temperature, the latent heat becomes more important. The *Ste* number (≈1.607)[51] indicates that, although latent heat release is significant, it does not dominate the heat flow during cooling in the thin channel.

Peclet number (*Pe*) is defined as the ratio of the rate of advection by the flow to the rate of diffusion of the same quantity driven by a gradient[51]. For Al alloy under HPDC conditions, the *Pe* is always at least 2 orders of magnitude greater than one, implying a strong thermal boundary layer.

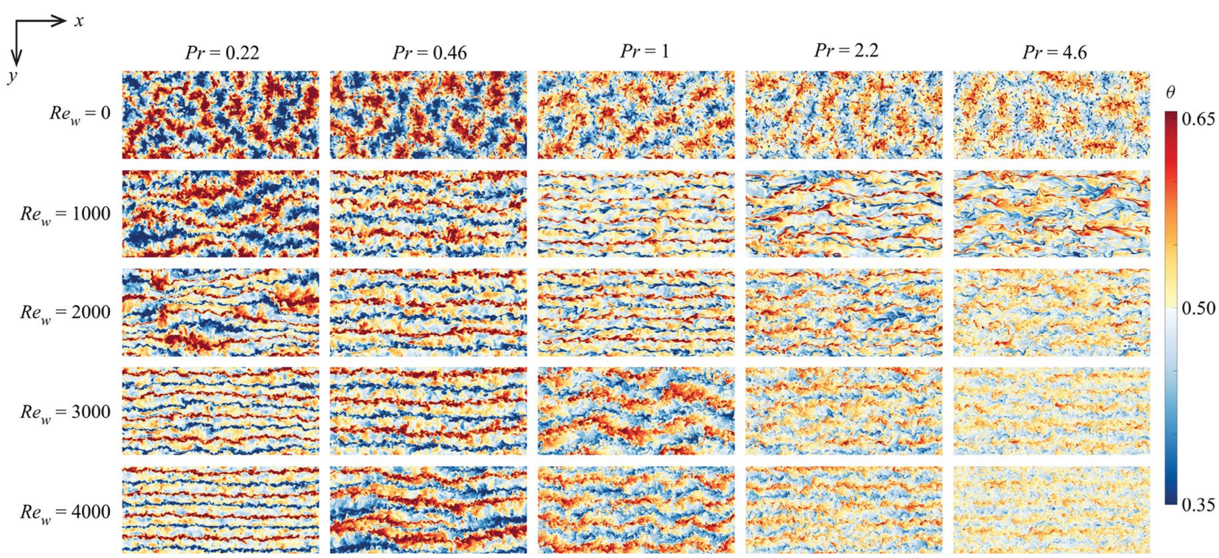

Fig. 10: Snapshots of the temperature field for a subdomain of the parameter space. The applied wall shear is in the *x* direction, while *y* is the spanwise coordinate, Re_w is the wall *Re* number, and θ is the normalized temperature[154]

The *Pe* number (≥100) suggests that heat advection always dominates the heat conduction, which indicates that heat advection in the center of thin walls has a significant influence on fluidity.

2.3.2 Transition from turbulent to laminar flow

The calculation of the *Re* indicates that the fluid initially enters the die in a turbulent state. As solidification progresses, the viscosity increases and the velocity decreases, leading to a transition toward a flow regime characterized by intermediate conditions. Eventually, the flow stabilizes into a laminar state (Fig. 11). This transition from turbulent to laminar flow forms the basis for the three stages involved in developing a numerical model. The Navier-Stokes equations govern the behavior of conventional fluids, which flow only in response to externally imposed body forces, stress, and pressure gradients[78]. However, boundary-generated active stresses may also have influence on fluidity. In systems like Rayleigh-Bénard convection, continuous energy injection through macroscopic external boundaries drives the flow[157]. In isotropic liquid, bounding surfaces disrupt local symmetry, aligning constituent particles and generating surface stresses. These changes will occur during the transition from turbulent to laminar flow, which is expected to take a few milliseconds.

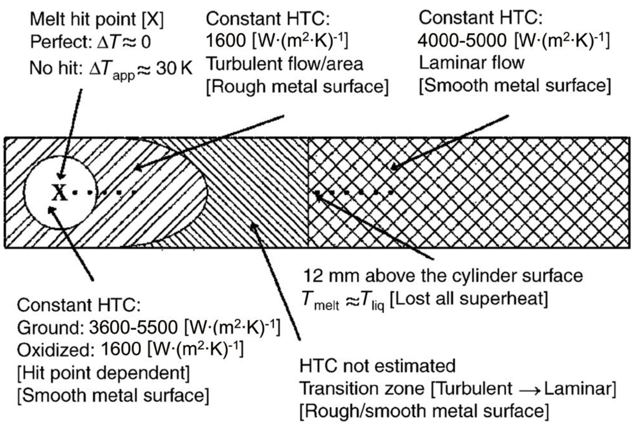

Fig. 11: Schematic of the transition from turbulent to laminar flow[17]

3 Flow choking mechanism

3.1 Solidification process perspective

For pure metals and eutectic alloys, solidification occurs at melting or eutectic point and progresses through the advance of a planar interface[158] from the die wall. This process, termed skin freezing[4], continues until the channel is ultimately choked by solidification (Cut-off mechanism). Due to solidification takes place from the die wall toward the center, grains in these materials typically form as columnar dendrites, as illustrated in Fig. 12(a). In planar solidification, the solidification front advances smoothly from the channel wall. This mode ensures high fluidity as the interface between the solid and liquid metal remains uninterrupted and stable. The fluidity behavior of ternary Al alloys closely resembles that of binary alloys. Maximum fluidity values are observed at compositions corresponding to eutectic valleys and wells in the ternary phase diagram, while minimum values occur along phase ridges[95].

Unlike pure metals and eutectic alloys, the solidification process of alloys within the critical solidification interval, such as some hypoeutectic Al-Si alloys, involves mixed growth [Fig. 12(b)]. In this mode, liquid, solid, and pasty layers frequently coexist within the casting cross-section[87, 101]. For alloys with mixed solidification process, fluidity is generally inversely proportional to the solidification range[83]. This mode represents intermediate solidification behavior (block mechanism), where both planar interface growth and mushy zone formation occur, depending

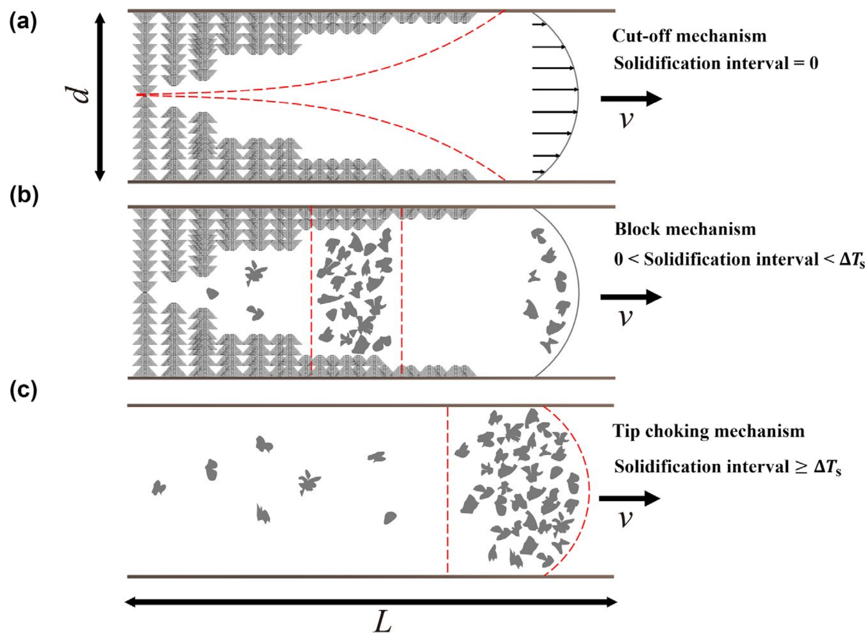

Fig. 12: Flow choking caused by three distinct solidification processes from solidification process perspective: (a) cut-off by columnar dendrites; (b) blockage by columnar and equiaxed dendrites; (c) tip choking by equiaxed dendrites

on local casting conditions such as temperature gradients, alloy composition, and gate speed.

For solute-rich alloys with a wide solidification interval, equiaxed crystals continuously nucleate within the melt during solidification[159]. These nucleates are carried by the melt and gradually accumulate at the fluid head, eventually blocking the flow channel and stopping the flow. The phenomenon termed tip choking mechanism, as shown in Fig. 12(c). It was previously considered the dominant solidification process when additional grain refiners were introduced[148].

The grains in most of alloys used in HPDC typically exhibit equiaxed dendritic structures with irregular growth surfaces, which can decrease the fluidity. This reduced fluidity can be attributed to phenomena like constitutional undercooling, which promotes independent crystallization within the main liquid mass, leading to the presence of free crystals. These free crystals lead to the formation of a mushy zone in alloys with a large solidification interval. Consequently, the fluidity of pure metals and eutectic alloys is generally much greater than that of alloys with a large solidification interval. In pure Al, fluidity starts high, decreases with the addition of alloying elements as the crystallization range widens, and increases again as the alloy composition approaches the eutectic point[122]. This behavior aligns with the fluidity changes discussed in Section 2.2.1.

3.2 ESCs perspective

ESCs are considered to be grains that are detrimental to the fluidity under HPDC process[19]. The area fraction of ESCs increased from surface to center with its morphology changed from fine globular shape into coarse dendritic shape[33]. The classical theory of alloy fluidity, based on the solidification mode at the leading tip of the stream, was developed primarily for gravity casting conditions [Fig. 13(a)]. However, the same theory does not apply to HPDC conditions. Die filling during HPDC is usually completed within a fraction of a second, such that the temperature drop at the leading tip of the stream is negligible. Therefore, the choking of flow is not affected by solidification phenomena at the flow front.

The A380 alloy was used to investigate the effects of ESCs under HPDC conditions[19]. A significant amount of ESCs are observed in the runner of the casting system. These ESCs form in the shot sleeve and are transported into the runners and casting. Under the influence of the Magnus effect[160], ESCs can create a segregation core, leaving a thin ESCs-free zone near the surface of the flow channel. They gather in the center, forming a rigid dendritic network that chokes flow in the narrower sections of the fillling and gating system [Fig. 13(b)]. Additionally, ESCs reduce the viscosity and permeability of the mushy zone, leading to an increased pressure drop as molten metal flows through it. When the pressure drop equals or exceeds the driving pressure, the melt flow ceases.

Dendrites can be characterized by three length scales: grain size, primary dendrite arm spacing, and secondary dendrite arm spacing (SDAS)[161]. Among the scales, SDAS is strongly influenced by cooling rates and local solidification time[162], making it an important indicator of where dendrites form within a HPDC system. The SDAS ranges from approximately 10 to 30 μm for ESCs[19]. Iron-containing intermetallic phases, such as α or β, are pushed by dendrites into interdendritic regions and coexist with eutectic phases[163]. However, the volume fraction of these intermetallic phases is minimal, making them unlikely to obstruct the flow during the die-filling process. Additionally, these intermetallic eutectic phases form later in the solidification process. When the solid fraction exceeds 0.8[163], these phases begin to precipitate in large quantities, forming defect bands[164]. By this point, however, the flow has already been choked.

Three choking locations associated with ESCs are identified[19]. The first is entrance choking, where flow choking occurs at the runner entrance due to ESCs, typically at solid fractions around $f_s \approx 0.6$, as the plunger struggles to push molten metal into the runner. The second is thinner section choking, where ESCs obstruct flow at or near narrower sections of the gating system, occurring at $f_s \leq 0.6$. The third is flow channel choking, where a pressure drop arises due to primary ESCs in the flow channels. In this scenario, even small fractions of solidifying material from the shot sleeve can form a rigid dendritic network that significantly increases flow resistance and impedes die filling.

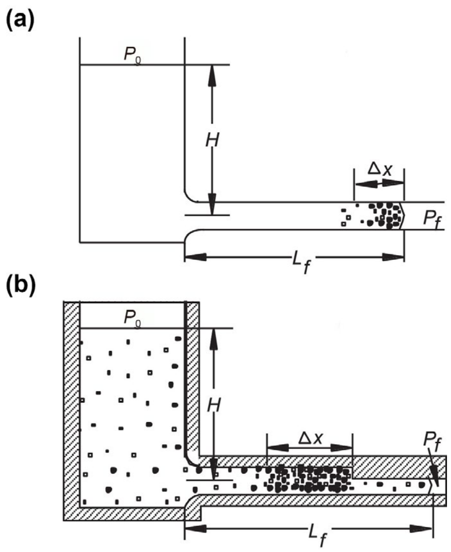

Fig. 13: Flow choking mechanism from ESCs perspective: (a) choking at the flow front in gravity casting and (b) choking at the variable cross section in HPDC with three choking locations[3]

3.3 Peeling perspective

From ESCs perspective, the flow resistance is caused by the accumulation of ESCs at the cross-section, however, the absence of significant cross-sectional changes in the runner undermines its persuasiveness. Haga et al.[80] proposed a different mechanism using Al-Si alloy for the flow choking under HPDC process. They attributed the resistance and changes in fluidity to the peeling and growth of the solidified layer. As shown in Fig. 14(a), based on Si content, the Al-Si alloy can be divided into two distinct regions, A and C, with an inflection point, B. Region C exhibits a higher Si content, while Region A is characterized by a lower Si content.

The adhesion time of the solidified layer decreases with lower Si content, as the latent heat of the Al-Si alloy decreases accordingly. When the Si content drops below 6%, the solidified layer becomes thinner than under higher Si conditions and exhibits a peeling pattern similar to that shown in Fig. 14(b). The latent heat of alloy reduces, accelerating the cooling and shrinkage of the solidified layer. This process leads to the earlier formation of a gap between the solidified layer and the die surface, increasing interfacial thermal resistance[165] and reducing heat transfer from internal liquid to die surface. This phenomenon explains the increase in fluidity observed when the Si content falls below 6%.

For Al-Si alloys with Si content of 6%, the adhesion pattern of the solidification layer aligns with Fig. 14(c). This phenomenon occurs because, when the Si content reach the inflection point B, the increased latent heat of the Al-Si alloy slows the cooling rate of the solidified layer[166]. Consequently, the subsequent melt can fill the gaps caused by shrinkage, preventing the solidified layer from peeling off beyond the inflection point B. However, in this case, the Si content remains low, resulting in a relatively small latent heat of the alloy. Additionally, no insulating layer forms between the solidified layer and the die surface. Consequently, the interfacial thermal resistance related to the solidification of the internal metal liquid is minimized, leading to rapid solidification of the internal metal and choking the flow[167].

In Region C, the fluidity of the alloy improves as the Si content increases, as illustrated in Fig. 14(d). This is attributed to the rise in the latent heat of alloy with increasing Si content[93], which reduces the cooling rate of the solidified layer. Consequently, the rate of solidified layer thickening decreases, leading to an enhancement in fluidity.

The peeling assumption demonstrates that in regions with lower Si contents (to the left of the inflection point), the peeling of the solidified layer from the die is the dominant factor. In contrast, in regions with higher Si contents (to the right of the inflection point), latent heat plays a more significant role. However, variables such as wall thickness, die temperature, and shot speed influence the formation and peeling of the solidified layer. For instance, higher die temperatures[168] reduce the rate of solidified layer thickening, leading to enhanced fluidity. Therefore, it is necessary to comprehensively consider the influence of casting variables on peeling.

3.4 Shear force perspective

Currently, the mechanism of shear-induced choking has not been discussed in the literature. However, the high gate speed and complex die geometry make the effects of shear forces particularly significant in HPDC. Therefore, we briefly review the effects of shear force here.

The Navier-Stokes equations indicate that traditional fluids such as metals will flow only in response to external pressure gradients[169]. In this condition, energy cascades through multiple length scales before being dissipated in the turbulent fluid[170]. Kurotani et al.[157] researched the influence of shear on liquid flow through the novel physical mechanism of shear-induced cavitation and gas-layer formation near solid surfaces. They found the coupling between shear flow, density fluctuations, and viscosity variations leads to a significant reduction in flow resistance through shear-induced slippage

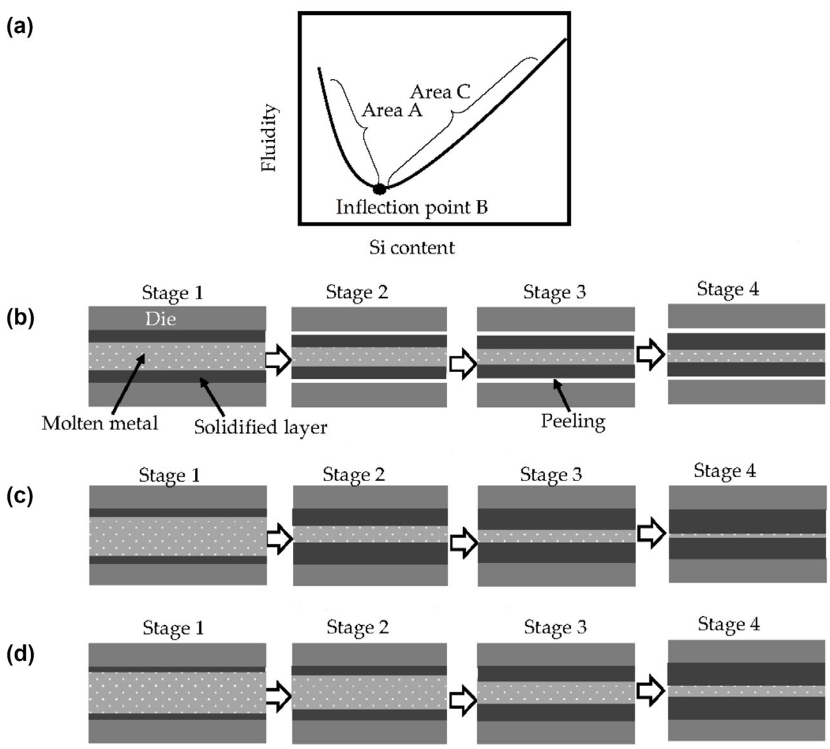

Fig. 14: Flow choking mechanism in peeling perspective: (a) fluidity of Al alloys with varying Si content, divided into three regions; (b) choking mechanism when Si content is below the inflection point; (c) choking mechanism at the inflection point of Si content; (d) choking mechanism when Si content exceeds the inflection point[80]

mechanisms, applicable across different liquid systems.

Near the wall, shear flow enhances density fluctuations due to the dependence of viscosity on density. At high shear rates, these fluctuations destabilize the liquid, promoting gas layer formation near the solid surface. When the shear rate surpasses a critical threshold, dissolved gas in the liquid aggregates, forming bubbles on the surface. These bubbles reduce friction and facilitate sliding. As shown in Fig. 15(a), when the shear rate is zero ($\dot{\gamma}$=0), intrinsic density fluctuations near solid surfaces arise due to boundary conditions influenced by the contact angle θ. When the shear rate increases to $\dot{\gamma}$=0.01, density fluctuations near the wall are further enhanced [Fig. 15(b)] compared to the quiescent state.

Density fluctuations are inherently amplified near the wall, even in a quiescent state, regardless of the wall properties[171]. The equilibrium amplitude of thermal density fluctuations is governed by the interplay between the strength of thermal fluctuations and the compressive resilience against them. For liquids with high viscosity[172], spontaneous shear-induced slippage can take place even at a low shear rate. This slip causes the solute-rich liquid to segregate, leading to positive macrosegregation (defect bands) during solidification[57, 173]. These defect bands create large area holes[23] at the flow end, which can develop into significant cracks under shear forces[174], finally causing the flow choking.

4 Algorithms for predicting fluidity

In the late 20th century, advancements in ML[175] and artificial neural networks[176] (ANNs) sparked interest in exploring defects and HPDC process parameters. However, limited computing power quickly shifted focus to other research areas. Recently, with significant improvements in computational capabilities (e.g., GPU) and the widespread adoption of generative artificial intelligence (AI), algorithm-based prediction and optimization of fluidity and process parameters have re-emerged as a key research focus[21, 177-179].

In recent years, data-driven process parameter optimization has been successfully implemented[177]. Additionally, integrating ML with computed tomography (CT) data to predict voids and cracks has become a mainstream research focus[180]. Convolutional neural networks (CNNs)[181] and graph neural networks (GNNs)[182] show great potential for handling the large volumes of image data generated by CT.

Figure 16 illustrates the average categorized citations of publications from January 2020 to January 2025, with node size scaled by the occurrence per source. The data, sourced from the Web of Science, was manually screened to include 6664 articles. Keywords with a frequency of more than 25 occurrences were selected as the explicit node data. It can be found that the articles related to ML and ANNs have been cited more

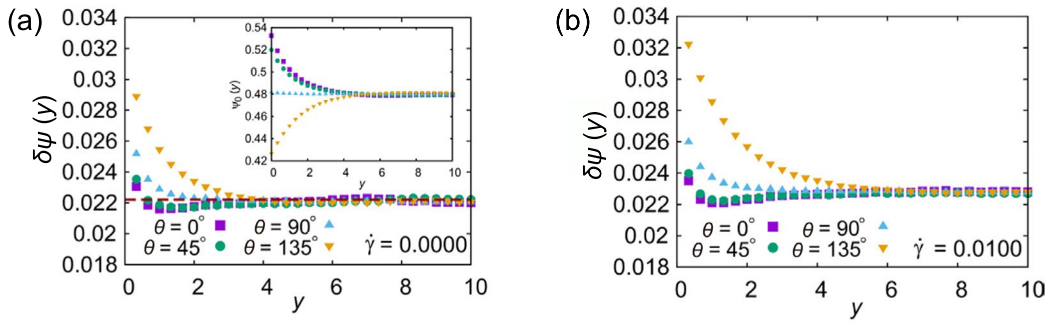

Fig. 15: Density fluctuations near the wall under quiescent and shear conditions: (a) amplitude of density fluctuations near the boundary wall at $\dot{\gamma}$=0. The inset shows the average density profile near the boundary wall; (b) amplitude of density fluctuations near the boundary wall at $\dot{\gamma}$=0.01[157]

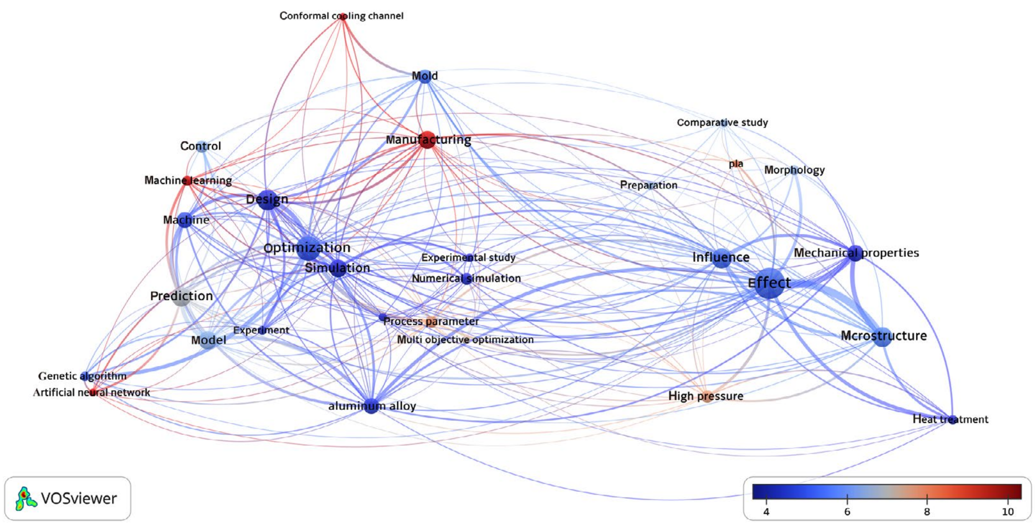

Fig. 16: Visualization of the average categorized citations of publications on 'die casting' and 'aluminum alloy algorithms' from 2021.01 to 2025.01, red color indicates a high frequency of citations (VOSviewer[183])

times but published less in recent years. Table 1 summarizes the objectives, training data sources, algorithms employed, and innovations in recent literature. The following section will provide a discussion on the applications of ML, genetic algorithms (GA), and fuzzy algorithms for the field of HPDC.

4.1 Machine learning

Machine learning (ML) methods applicable to small datasets include regression, classification, clustering, natural language processing, time series analysis, and reinforcement learning. Among these, regression is most commonly applied in materials science[203]. The basic process of modeling and prediction using ML is shown as Fig. 17, including data collection, data pre-processing, algorithm selection, distinguishing between training and validation sets, and model modification.

The ML process begins with collecting or generating labeled data, followed by cleaning it to ensure accuracy and relevance. Afterward, an appropriate algorithm is selected, and the data

Table 1: Typical algorithms used in the HPDC field and the corresponding data source and innovations

Objectives	Data source	Algorithms	Innovations	Source
Defects	Production data	XGBoost classification	Hyperopt library	[184]
Yield strength	Reviewed literature	Decision trees, Extra tree, RF, XGBoost (best)	Comparison of different models	[185]
Strength	Al ASM Handbook and reviewed literature	SVR-RBF, RF, DNN, and XGBoost (best)	Multi-objective genetic algorithm optimization	[186]
Mechanical properties	Experiments	CNNs	Model couplings	[187]
Fluidity	Simulation results	ANNs	Different numbers of neurons in the hidden layer	[21]
Impact toughness	Openaccess steel database	LR, SMOreg, M5P, MP, KNN, and RF (best)	Selected features was obtained by using a SR method based on GA.	[188]
Defects and solidification time	Simulation results	ANNs	GA optimisation	[189]
HPDC parameters	Reviewed literature	Polynomial regression, SVM/SVC	–	[177]
Injection speed	Simulation results	BPNN	Neural network PID controller	[190]
HPDC parameters	Production data	logistic regression, RF, XGBoost, gradient boost, ANN	Principal component analysis	[191]
HPDC parameters	Production data	CNNs	Combine sensor signals to generate RGB image	[181]
Defects	Production data	XGBoost classification	Associating the X-ray and HPDC machine	[192]
Surface defects	Production data	Computer vision	–	[193]
Gating system	Reviewed literature	MLP and CNNs	Multimodal models contain both text and image data	[178]
Microhardness, tensile strength, and elongation	Experiments	Response surface and NSGA-2	Combination algorithm	[194]
Porosity	Experiments	Fuzzy algorithm	GA and SA optimization	[195]
Interfacial heat transfer coefficient	Experiments	Decision tree, MLR, ANNR (best)	–	[196]
HPDC parameters	Experiments	Co-Evolutionary Algorithm	Improved hybrid particle swarm optimization	[197]
HPDC parameters	Experiments	GA and Fuzzy algorithm	GA optimization	[198]
Hardness, porosity and surface roughness	Experiments	BPNN	Comparison of BPNN and statistical models	[199]
HPDC parameters	Experiments	Neural network	Levenberg-Marquartdt training algorithm	[200]
Porosity	Experiments	GA	MLR analysis	[201]
HPDC parameters	Experiments	Fuzzy algorithm	Integrated grey relational analysis	[202]

Note: XGBoost – eXtreme Gradient Boosting; RF – random forest algorithm; SVR – support vector regression; RBF – radial basis function; DNN – deep neural network; LR – linear regression; SMOreg – sequential minimal optimization for regression; M5P – M5 tree model; MP – multi-layer perceptron; KNN – K-nearest neighbors; SVM – support vector machine; SVC – support vector classifier; MLP – multilayer perceptron; NSGA-2 – non-dominated sorting genetic algorithm 2; ANNR – active nearest neighbor regressor; SR – symbolic regression; SA – simulated annealing; BPNN – back-propagation neural network; GA – genetic algorithm; MLR – multiple linear regression

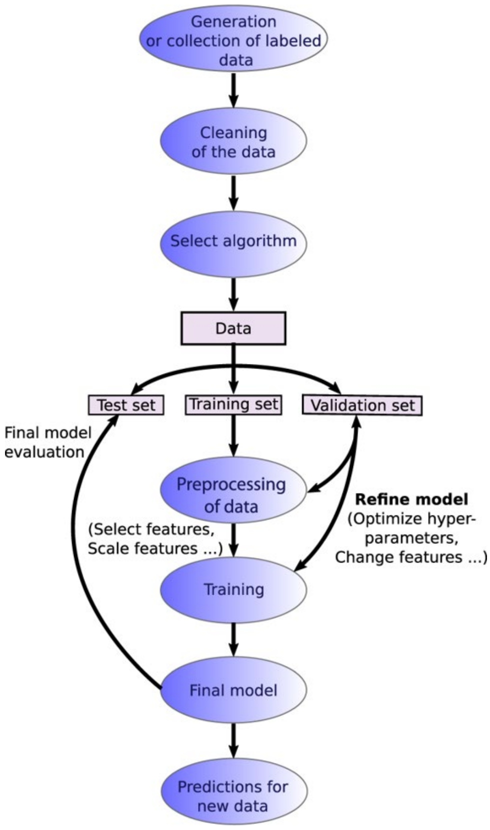

Fig. 17: Basic process of ML[204]

is split into training, validation, and test sets. The data are then preprocessed, including tasks like feature filtering and scaling, to prepare it for model training. The model is trained using the training set and refined iteratively by optimizing hyperparameters and modifying features based on validation set performance. Once the model is finalized, its performance is evaluated on the test set, and it is deployed to make predictions on new, unseen data.

Currently, increasing research focuses on predicting and optimizing material properties and developing new alloys through composition design. While this approach can also be applied to fluidity, there is limited literature on this topic. Therefore, the following section will mainly review prediction methods and specific steps, because the input data can be adjusted based on the desired performance.

Figure 18 outlines the detailed steps for designing alloys with a high specific modulus and specific strength[205, 206]. Features filtering is mainly about removing the noisy and redundant irrelevant feature candidates from feature space, thus reducing the dimensionality of the input without losing important information for model building. Feature filtering methods are numerous, but the first step typically involves using the pearson correlation coefficient (PCC)[207]. PCC is the measure of the linear correlation of two features to eliminate the redundant features [Fig. 18(a)]. It is based on:

$$r_{xy} = \frac{\sum_{i=1}^{n}(x_i - \bar{x})(y_i - \bar{y})}{\sqrt{\sum_{i=1}^{n}(x_i - \bar{x})^2}\sqrt{\sum_{i=1}^{n}(y_i - \bar{y})^2}} \tag{12}$$

where r_{xy} is the degree of correlation, n is the sample size, x_i and y_i are the individual sample points indexed by i, $\bar{x}$ and $\bar{y}$ are the sample means of x and y, respectively. r_{xy} has a value between −1 and 1, and positive r means that the two features are positively correlated, while a negative r means that the two features are negatively correlated. A value of R was set as the feature filtering threshold, when $r_{xy}>R$, the highly-correlated feature x and y are separately removed from the feature space.

The second filtering method is the recursive feature elimination (RFE)[208], which uses a base ML model for multiple rounds of training, and after each round of training, the feature corresponding to the smallest model error is eliminated and the next round of training is performed on the new set of features until the model error no longer maintains at a low level but increases significantly.

Next step of feature filtering is performed using the best subset selection (BSS) method[209], combining the chosen ML algorithms with default model parameters. Cross-validation is used for validation, and R^2 serves as the evaluation metric. The BSS method builds 2n models (n is the number of remaining feature candidates) by creating the exhaustive combinations of features and putting them in the ML model as input, which finally obtains several features that have the greatest impact on the target properties by comparing the model errors [Fig. 18(b)].

Algorithm comparison can be performed either before or after the BSS process. Following this step, only the most important features are retained, and the best algorithm is selected based on the lowest mean squared error (MSE) and the highest R^2 value. The result of regression is shown as Fig. 18(c), the results from the training set and prediction set reflect the accuracy and generalization ability of the model. After iterative hyperparameter optimization and feature selection, the final model is established. It is important to note that feature selection should not rely solely on feature filters but also requires expert knowledge (e.g., solidification theory) to guide the selection process[205].

The final step is to use the established model to predict unknown datasets and provide an accuracy assessment [Fig. 18(d)]. In most cases in materials science, the performance of interest serves as the prediction indicator. ML has been applied to predict strength, fatigue performance, fracture toughness, thermal conductivity, and electrical conductivity[185, 210, 196]. However, predicting fluidity under HPDC conditions remains in its early stages. Currently, some ML methods are available for optimizing process parameters[189] to achieve better casting performance, with broader applications anticipated in the future.

4.2 Deep learning

Deep learning, a branch of ML, is mainly utilized for processing large datasets (typically over 100,000 samples). While diffusion and transformer models currently dominate research in image and text domains, traditional ANNs remain widely used for predicting defects and casting variables. Insufficient fluidity often results in shrinkage defects. Identifying these defects allows for reliable measurements, indirectly reflecting the fluidity. Optimizing casting variables enables the coupled regulation of mechanical properties and fluidity during the process.

Parlak et al.[211] explored the application of deep learning for detecting internal defects in Al components under HPDC using X-ray imaging [Fig. 19(a)]. By employing modern object detection algorithms like YOLOv5, trained on a novel open-access X-ray image dataset and enhanced with techniques such as contrast adjustment and data augmentation. The system achieves high accuracy in identifying defect types like shrinkage and gas holes. Bhat et al.[212] provided an overview of deep learning techniques used to detect defects in Al alloys under HPDC process. Traditional non-destructive testing methods, such as X-ray and ultrasonic testing, are effective but can sometimes fail to detect minute flaws. Deep learning, especially CNNs, enhances defect detection accuracy using labeled radiographic images to identify porosity, shrinkage, and cracks[198].

Additionally, a novel approach was developed to construct the model of HPDC process. The model is based on neural networks[199]. Forward mapping [Fig. 19(b)] predicts output characteristics (e.g., fluidity) based on known input parameters (e.g., fast shot speed). Back-propagation neural networks (BPNN) use iterative error minimization for such nonlinear predictions[213]. Reverse mapping, in contrast, estimates input settings required to achieve desired outputs. Together, these approaches, applied here to HPDC, offer process optimization.

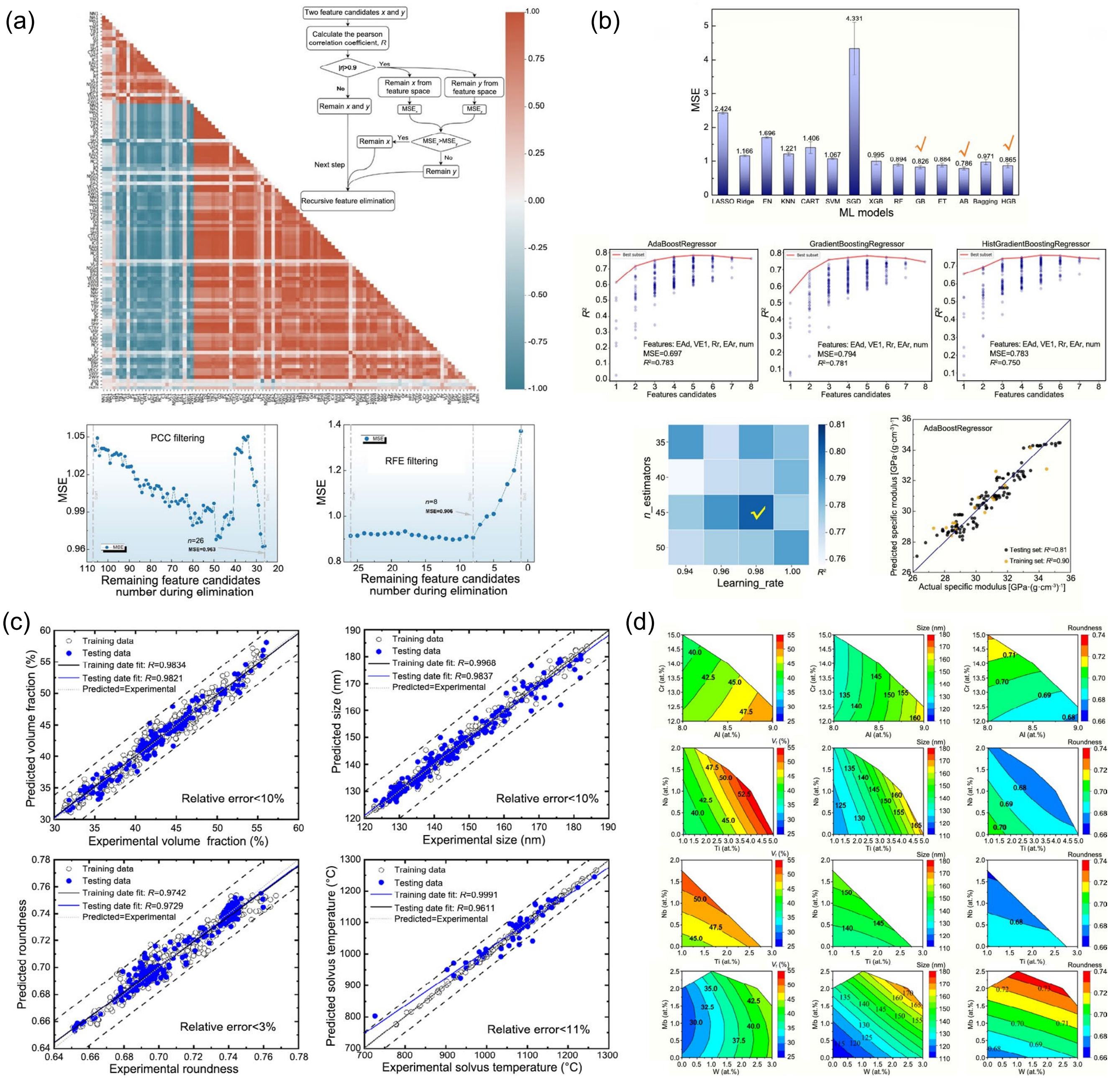

Fig. 18: Detailed process of modeling and prediction using ML: (a) two-step feature filtering method including PCC and RFE[205]; (b) algorithm selection and BSS feature filtering, including correlation analysis and regression testing[205]; (c) visualization of the training and test sets and the prediction accuracy of the model[206]; (d) apply the model to an unknown test set and make performance predictions[206]

Furthermore, integrating visual, textual, and numerical data into a regression model could achieved high prediction accuracy for parameters[178]. This multimodal ML approach requires more complex input and poses challenges in data preprocessing, but it can improve model accuracy if successful.

Figure 19(c) illustrates the schematic use of long short-term memory recurrent neural networks as virtual sensors for pressure and temperature in HPDC[214]. Physical cavity sensors are expensive and have limited lifetimes, making virtual sensors a promising alternative. Using data from 233 training cycles and 99 test cycles, the models achieve great accuracy for cavity temperature and cavity pressure, especially during the filling and solidification phases. However, this algorithm prediction declines over longer time intervals due to casting distortions after solidification.

4.3 Genetic algorithms

Genetic algorithm (GA) is optimization techniques inspired by natural selection and genetics[215]. They work by simulating the evolutionary process, where potential solutions to a problem (called individuals) are encoded as chromosomes. Through iterative processes of selection, crossover (recombination), and mutation, GA can search for optimal or near-optimal solutions.

GA is also known as stochastic sampling methods, solving challenging problems where objective functions have undesirable properties such as being multi-modal, discontinuous, or non-differentiable[197]. GA is particularly suited for problems with large search spaces or non-linear variable relationships. The mutation rate, often set at around 1%[216], falls within the typical range for these algorithms. However, a notable drawback is their higher computational effort compared to traditional optimization methods.

Tsoukalas[201] used GA to optimize the process parameters in multivariable linear regression model in HPDC. The input variables are holding furnace temperature, die temperature, slow shot speed, fast shot speed, and IP.

4.4 Fuzzy algorithm

The most important characteristic of fuzzy algorithm is its capability of modeling and utilizing knowledge from expert in a linguistic way[217]. There are basically four components in the fuzzy logic system which are: fuzzifier, knowledge base, inference engine, and defuzzifier.

Cica et al.[195] used Mamdani-type fuzzy inference algorithm to predict the percentage of porosity in aluminum HPDC. These input and output process variables were fuzzified and represented

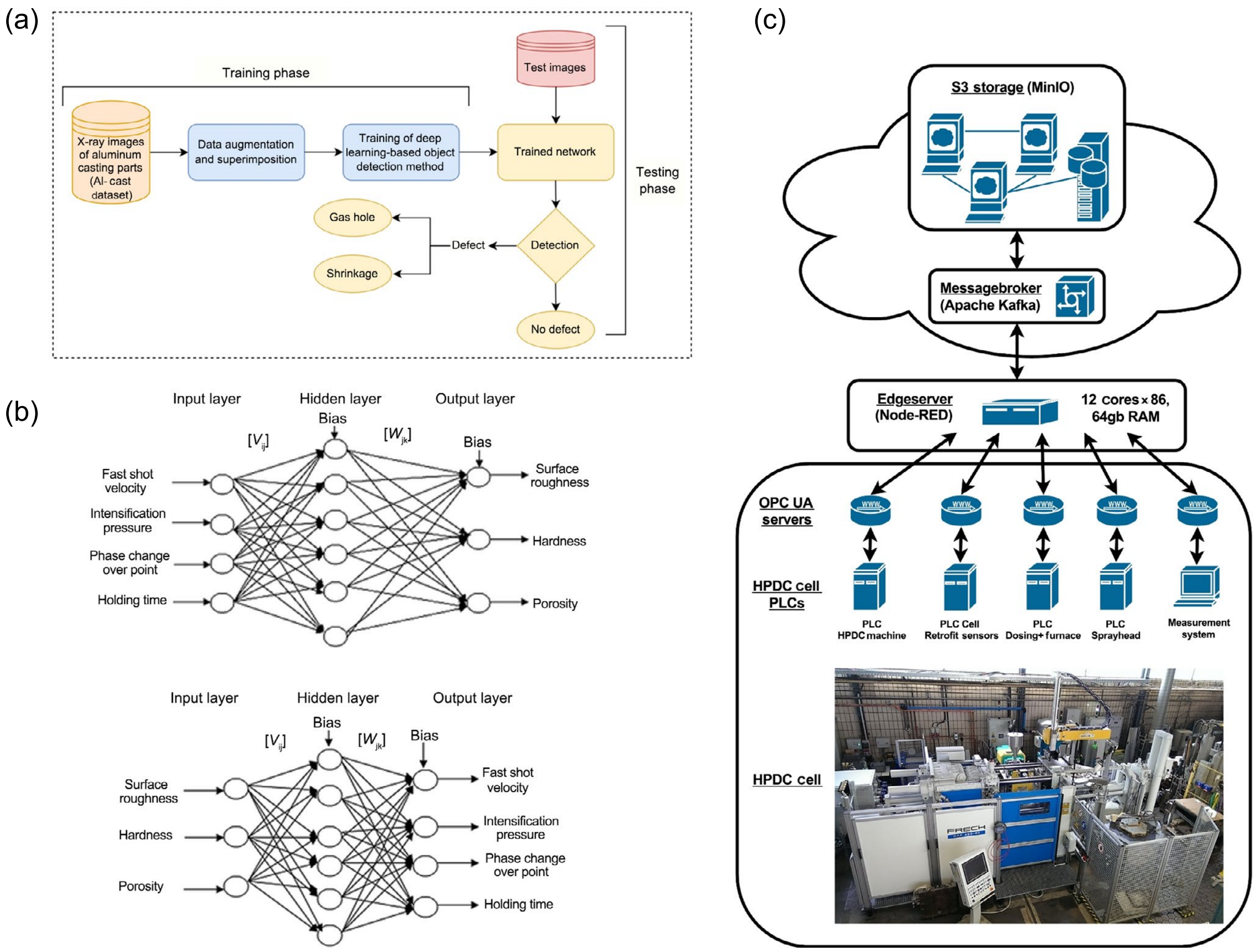

Fig. 19: Detailed process of modeling and prediction using deep learning: (a) proposed model to detect defects in Al casting part[211]; (b) structure of neural network used for forward mapping and reverse mapping[199]; (c) infrastructure to capture and persist the ML data set, which can be used for time series forecasting[214]

by means of appropriate membership functions which could be optimized by GA and simulated annealing algorithm[206].

Another fuzzy model was developed with five inputs and one output to represent HPDC defects[198]. The input variables included solidification time, melting temperature, filling time, inoculation pressure, and plunger velocity. A GA search heuristic was employed to identify optimal combinations of machining parameters, as GA proves to be more effective for optimization compared to traditional statistical methods. Furthermore, an integrated algorithm combining grey relational analysis and fuzzy logic was also explored[202]. The grey aspect represents primitive data with poor, incomplete, and uncertain information, while the incomplete relationships among these data are referred to as grey relations. The analysis identified die temperature and injection pressure as the most significant casting variables.

5 Summary and outlook

In recent years, interest in the fluidity of Al alloys in the HPDC state has grown, as it directly influences properties and the final size of castings. Improved fluidity enables the formation of large solid parts in a single process, reducing weight and meeting the demands of applications such as front engine compartment, rear floor panel, motor housing, and electric drive housing of EVs. Fluidity is an indicator for measuring the flow length under a set of narrow die filling conditions. The fluidity of molten metal is directly influenced by the shape and complexity of the casting. More complex geometries and thinner sections pose challenges to the ability to completely fill the die cavity, which may lead to defects such as cold shuts, shrinkage, and incomplete filling.

The significant progress in fluidity over the past decade has been driven by a deeper understanding of the impact of variables on fluidity, alongside continuous advancements in algorithms. This has proven highly beneficial for coupling studies of velocity field, temperature field, and microstructure field in the HPDC process. Various variables directly or indirectly influence the fluidity in the HPDC state. These variables can be classified into three categories based on their sources: casting variables, metallurgical variables, and flow variables. Among them, casting variables and metallurgical variables are direct variables, while flow variables are indirect variables. Generally, established flow models typically incorporate empirical parameters derived through data fitting. However, to enhance predictive accuracy and refine the models, it is essential to understand how variables influence these empirical parameters. Firstly, casting variables refer to processing parameters that can be directly adjusted using HPDC equipment. For example, higher shot speeds and greater IP can delay the formation of ESCs dendrite networks and have positive influence on fluidity. Secondly, metallurgical variables pertain to the intrinsic properties of the molten metal. Fluidity can be further enhanced by optimizing alloying elements near the eutectic composition, incorporating elements with high latent heat for micro-alloying, selecting an appropriate superheat, and implementing effective melt cleaning treatments. Thirdly, flow variables such as *Re*, *Pr*, *Nu*, *Ste*, and *Pe*, reflect the flow state and the position of the heat transfer layer during the flow process.

Various mechanistic explanations exist for flow choking under HPDC conditions. Identifying the location of choking primarily relies on techniques such as microscopy, CT, and synchrotron radiation observation. However, extensive experimental comparisons are often required, posing a significant challenge. Therefore, current research is basically based on inference and empirical explanation. Factors such as alloy composition, solidus temperature, the formation of dendrite networks, and wall peeling have been proposed, though no consensus mechanism has been established. A deeper understanding of the flow choking mechanism could enable the adjustment of variables through negative feedback. Finally, few studies specifically focus on using algorithms to predict fluidity. Current research predominantly emphasizes optimizing casting variables and predicting defects such as porosity, both of which can indirectly reflect fluidity. For algorithms, the primary approaches that integrated GA with other techniques were used several decades ago. In recent years, the rise of ML and advances in computational power have made AI methods increasingly popular, though their application in this field remains limited.

To gain a deeper and more comprehensive understanding of the influence of various variables on alloy fluidity under HPDC process, further research is needed on underlying mechanisms, including the interactions among multiple components, the flow choking process, and previously unobserved flow-related microstructural evolution. Simultaneously, it is essential to refine and enhance algorithm-based numerical models. The opportunities and challenges can be summarized as follows:

(1) Measuring fluidity requires an experimental carrier, but standardized methodologies for fluidity test die design remain inconsistent. Developing a standardized die is essential to ensure repeatable and reliable fluidity measurements. Building on this, the mechanism of how variables affect fluidity under HPDC conditions can be further studied.

(2) The flow choking mechanism and model should be considered together. Currently, the flow choking position in HPDC is assumed to be at the variable cross-section, though this has not been experimentally verified. The model can be used to calculate the flow length, with the resulting distance helping to identify the flow choking point or the solidification point where significant changes in microstructure occur. Three-dimensional reconstruction technologies, such as CT scanning, can be used for experimental verification.

(3) The development of integrated die casting technology is closely linked to metal fluidity, making the creation of new high fluidity alloys a key focus. The application of AI algorithms in material design has also emerged as a critical research direction. Establishing a fluidity-related database and integrating sensors in factory environments for time series prediction can provide foundations for model development.

Acknowledgments

This work was financially supported by the National Key Research and Development Program of China (Grant No. 2022YFB3404201) and the National Natural Science Foundation of China (Grant No. 52175335).

Conflict of interest

Prof. Shou-mei Xiong is an EBM of *CHINA FOUNDRY*. He was not involved in the peer-review or handling of the manuscript. The authors have no other competing interests to disclose.

References

[1] Wang L, Makhlouf M, Apelian D. Aluminium die casting alloys: Alloy composition, microstructure, and properties-performance relationships. International Materials Reviews, 1995, 40(6): 221–238.

[2] Niu Z C, Liu G Y, Li T, et al. Effect of high pressure die casting on the castability, defects and mechanical properties of aluminium alloys in extra-large thin-wall castings. Journal of Materials Processing Technology, 2022, 303: 117525.

[3] Han Q. A model correlating fluidity to alloy variables in hypoeutectic alloys. Acta Materialia, 2022, 226: 117587.

[4] Niu G, Wang Y, Zhu L, et al. Fluidity of casting Al-Si series alloys for automotive light-weighting: A systematic review. Materials Science and Technology, 2022, 38(13): 902–911.

[5] Dou K, Lordan E, Zhang Y, et al. A novel approach to optimize mechanical properties for aluminium alloy in high pressure die casting (HPDC) process combining experiment and modelling. Journal of Materials Processing Technology, 2021, 296: 117193.

[6] Liu Y X, Liu Y C, Akhtar S, et al. Thermal conductivity of binary Al alloys with different alloying elements. Journal of Alloys and Compounds, 2025, 1010: 177257.

[7] Berlanga-Labari C, Biezma-Moraleda M V, Rivero P J. Corrosion of cast aluminum alloys: A review. Metals, 2020, 10(10): 1384.

[8] Ducker C. ATG 2022 North American light vehicle aluminum content and outlook summary report. Aluminum Transportation Group, 2023.

[9] Flemings M C. Fluidity of metals-techniques for producing ultra-thin section castings. The British Foundryman, 1964, 57: 312–325.

[10] Wang Q G, Wang A, Coryell J. Ultra-large aluminum shape casting: Opportunities and challenges. China Foundry, 2024, 21(5): 397–408.

[11] Jiao X Y, Wang J, Liu C, et al. Influence of slow-shot speed on PSPs and porosity of $AlSi_{17}Cu_{2.5}$ alloy during high pressure die casting. Journal of Materials Processing Technology, 2019, 268: 63–69.

[12] Liu W N, Zhang W, Wang P Y, et al. Effect of slow shot speed on externally solidified crystal, porosity and tensile property in a newly developed high-pressure die-cast Al-Si alloy. China Foundry, 2024, 21(5): 11–19.

[13] Wang Q L, Xiong S M. Effect of multi-step slow shot speed on microstructure of vacuum die cast AZ91D magnesium alloy. Transactions of Nonferrous Metals Society of China, 2015, 25(2): 375–380.

[14] Jalili N A, Akhlaghi M, Ahmadi N M. Simulation and analysis of flow in the injection chamber of die casting machine during the slow shot phase. The International Journal of Advanced Manufacturing Technology, 2009, 41(1–2): 31–41.

[15] Xie H, Wang J, Li Y, et al. Fast shot speed induced microstructure and mechanical property evolution of high pressure die casting Mg-Al-Zn-RE alloys. Journal of Materials Processing Technology, 2024, 331: 118523.

[16] Ravi K R, Pillai R M, Amaranathan K R, et al. Fluidity of aluminum alloys and composites: A review. Journal of Alloys and Compounds, 2008, 456(1–2): 201–210.

[17] Helenius R, Lohne O, Arnberg L, et al. The heat transfer during filling of a high-pressure die-casting shot sleeve. Materials Science and Engineering: A, 2005, 413–414: 52–55.

[18] Chen G C, Li X. Nanoparticle-enhanced castability of aluminum alloy 2024: Fluidity, hot cracking, and surface quality. Metallurgical and Materials Transactions: A, 2024(3): 761–773.

[19] Han Q, Zhang J. Fluidity of alloys under high-pressure die casting conditions: Flow-choking mechanisms. Metallurgical and Materials Transactions: B, 2020, 51(4): 1795–1804.

[20] Miller R A. Fluidity from a heat transfer perspective. NADCA Transactions, 2016.

[21] Teke Ç. Determination of flow distance of the fluid metal due to fluidity in ductile iron casting by artificial neural networks approach. Open Chemistry, 2022, 20(1): 1019–1028.

[22] Niu G, Wang J, Li J, et al. The formation mechanism of the chill fine-grain layer with high supersaturation and its influence on the mechanical properties of die casting Al-7Si-0.5Mg alloy. Materials Science and Engineering: A, 2022, 833: 142544.

[23] Gourlay C M, Laukli H I, Dahle A K. Defect band characteristics in Mg-Al and Al-Si high-pressure die castings. Metallurgical and Materials Transactions: A, 2007, 38(8): 1833–1844.

[24] Jiao X Y, Wang P Y, Liu Y X, et al. Effect of shot speeds on the microstructural framework and abnormal eutectic bands in a high pressure die casting hypoeutectic AlSi10MnMg alloy. Journal of Materials Processing Technology, 2024, 326: 118312.

[25] Li T, Song J, Zhang A, et al. Progress and prospects in Mg-alloy super-sized high pressure die casting for automotive structural components. Journal of Magnesium and Alloys, 2023, 11(11): 4166–4180.

[26] Luo A A, Sachdev A K, Apelian D. Alloy development and process innovations for light metals casting. Journal of Materials Processing Technology, 2022, 306: 117606.

[27] Liu Y, Xiong S. Research progress on thermal conductivity of high-pressure die-cast aluminum alloys. Metals, 2024, 14(4): 370.

[28] Zhang A, Li Y. Thermal conductivity of aluminum alloys – A review. Materials, 2023, 16(8): 2972.

[29] Wang Q L, Xiong S M. Vacuum assisted high-pressure die casting of AZ91D magnesium alloy at different slow shot speeds. Transactions of Nonferrous Metals Society of China, 2014, 24(10): 3051–3059.

[30] Wang B S, Xiong S M. Effects of shot speed and biscuit thickness on externaly solidified crystals of high-pressure die cast AM60B magnesium alloy. Transactions of Nonferrous Metals Society of China, 2011, 21(4): 767–772.

[31] Ma C, Yu W, Zhang T, et al. The effect of slow shot speed and casting pressure on the 3D microstructure of high pressure die casting AE44 magnesium alloy. Journal of Magnesium and Alloys, 2023, 11(2): 753–761.

[32] Jiao X, Liu C, Wang J, et al. On the characterization of microstructure and fracture in a high-pressure die-casting Al-10 wt%Si alloy. Progress in Natural Science: Materials International, 2020, 30(2): 221–228.

[33] Jiao X Y, Wang P Y, Liu Y X, et al. The characterization of porosity and externally solidified crystals in a high pressure die casting hypoeutectic Al-Si alloy using a newly developed ceramic shot sleeve. Materials Letters, 2024, 360: 136045.
[34] Garber L W. Theoretical analysis and experimental observation of air entrapment during cold chamber filling. Die Casting Engineer, 1982, 26: 14–22.
[35] Faura F, López J, Hernández J. On the optimum plunger acceleration law in the slow shot phase of pressure die casting machines. International Journal of Machine Tools and Manufacture, 2001, 41(2): 173–191.
[36] Kohlstädt S, Vynnycky M, Goeke S, et al. On determining the critical velocity in the shot sleeve of a high-pressure die casting machine using open source CFD. Fluids, 2021, 6(11): 386.
[37] Yu W B, Yuan Z H, Guo Z P, et al. Characterization of A390 aluminum alloy produced at different slow shot speeds using vacuum assisted high pressure die casting. Transactions of Nonferrous Metals Society of China, 2017, 27(12): 2529–2538.
[38] Adamane A R, Arnberg L, Fiorese E, et al. Influence of injection parameters on the porosity and tensile properties of high-pressure die cast Al-Si alloys: A review. International Journal of Metalcasting, 2015, 9(1): 43–53.
[39] Chavan R, Kulkarni P S. Die design and optimization of cooling channel position for cold chamber high pressure die casting machine. In: IOP Conference Series: Materials Science and Engineering, IOP Publishing, 2020: 012017.
[40] Kang H J, Jang H S, Oh S H, et al. Effects of gate system design on pore defects and mechanical properties of pore-free die-cast Al-Si-Cu alloy. Materials Today Communications, 2022, 31: 103673.
[41] Jiao X Y, Zhang Y F, Wang J, et al. Characterization of externally solidified crystals in a high-pressure die-cast AlSi10MnMg alloy and their effect on porosities and mechanical properties. Journal of Materials Processing Technology, 2021, 298: 117299.
[42] Yu W, Ma C, Ma Y, et al. Correlation of 3D defect-band morphologies and mechanical properties in high pressure die casting magnesium alloy. Journal of Materials Processing Technology, 2021, 288: 116853.
[43] Hu Q, Zhao H, Li F. Microstructures and properties of SiC particles reinforced aluminum-matrix composites fabricated by vacuum-assisted high pressure die casting. Materials Science and Engineering: A, 2017, 680: 270–277.
[44] Oertel H. Dynamics of fluid flow. In: Prandtl's essentials of fluid mechanics. New York: Springer, 2004: 63–216.
[45] Manninen M, Taivassalo V, Kallio S. On the mixture model for multiphase flow. 1996. https://api.semanticscholar.org/CorpusID:906342.
[46] Hu Q, Guo W, Xiao P, et al. Effects of fast shot speed and wall thickness on the microstructures and mechanical properties of the high pressure die-casting 6061-SiC composites. Metallurgical and Materials Transactions: B, 2021, 52(4): 2283–2293.
[47] Dou K, Lordan E, Zhang Y J, et al. A complete computer aided engineering (CAE) modelling and optimization of high pressure die casting (HPDC) process. Journal of Manufacturing Processes, 2020, 60: 435–446.
[48] Swaminathan C R, Voller V R. A general enthalpy method for modeling solidification processes. Metallurgical Transactions: B, 1992, 23(5): 651–664.
[49] Mansour N N, Kim J, Moin P. Near-wall k-epsilon turbulence modeling. AIAA Journal, 1989, 27(8): 1068–1073.
[50] Hirt C W, Nichols B D. Volume of fluid (VOF) method for the dynamics of free boundaries. Journal of Computational Physics, 1981, 39(1): 201–225.
[51] Monroe C A, Monroe A K. Predicting flow lengths in die casting including heat advection. In: Proc. Die Casting Congress & Exposition, Indianapolis, Indiana, 2012.
[52] Ma S, Huang C J, Chu Y, et al. Intensification feeding analysis of high pressure die casting process. In: Proc. Die Casting Congress, NADCA, 2020.
[53] Dargusch M S, Hamasaiid A, Dour G, et al. The influence of in-cavity pressure on heat transfer and porosity formation during high-pressure die casting of A380 alloy. JOM, 2020, 72(11): 3798–3805.
[54] Jin C K, Kang C G. Fabrication by vacuum die casting and simulation of aluminum bipolar plates with micro-channels on both sides for proton exchange membrane (PEM) fuel cells. International Journal of Hydrogen Energy, 2012, 37(2): 1661–1676.
[55] Bar-Meir G. On gas/air porosity in pressure die casting. Doctoral Dissertation, University of Minnesota, Minneapolis, 1995.
[56] Lee S G, Patel G R, Gokhale A M. Characterization of the effects of process parameters on macrosegregation in a high-pressure die-cast magnesium alloy. Materials Characterization, 2005, 55(3): 219–224.
[57] Otarawanna S, Gourlay C M, Laukli H I, et al. The influence of external mechanical stresses on agglomeration and bending of solidifying crystals. In: Materials Science Forum, Trans Tech Publications, 2010, 654–656: 1367–1372. https://doi.org/10.4028/www.scientific.net/MSF.654-656.1367.
[58] Niu X P, Tong K K, Hu B H, et al. Cavity pressure sensor study of the gate freezing behaviour in aluminium high pressure die casting. International Journal of Cast Metals Research, 1998, 11(2): 105–112.
[59] Cao L, Liao D, Sun F, et al. Prediction of gas entrapment defects during zinc alloy high-pressure die casting based on gas-liquid multiphase flow model. The International Journal of Advanced Manufacturing Technology, 2018, 94(1–4): 807–815.
[60] Niroumand B, Karbasi M, Bagherpoor-Torghabe H. Effect of gating system design on hot tearing susceptibility of A206 alloy. In: Proc. 11th International Foundrymen Conference: Foundry Industry – Significance and Future Challenges, 2011.
[61] Gašpár Š, Paško J, Majerník J. Influence of structure adjustment of gating system of casting mould upon the quality of die cast. Lüdenscheid: RAM-Verlag, 2017.
[62] Gašpár Š, Coranič T, Majerník J, et al. Influence of gating system parameters of die-cast molds on properties of Al-Si castings. Materials, 2021, 14(13): 3755.
[63] Sotiropoulos F, Abdallah S. The discrete continuity equation in primitive variable solutions of incompressible flow. Journal of Computational Physics, 1991, 95(1): 212–227.
[64] Vossel T, Wolff N, Pustal B, et al. Influence of die temperature control on solidification and the casting process. International Journal of Metalcasting, 2020, 14(4): 907–925.
[65] Watari H, Nishida S, Haga T, et al. Effect of casting conditions on fluidity of aluminum alloy in die casting. In: JSME 2020 Conference on Leading Edge Manufacturing/Materials and Processing, American Society of Mechanical Engineers, 2020.
[66] Swartz E T, Pohl R O. Thermal resistance at interfaces. Applied Physics Letters, 1987, 51(26): 2200–2202.
[67] Sinha N K, Choudhary I N, Singh J K. Influence of mold material on the mold stability for foundry use. Silicon, 2022, 14(6): 2895–2904.
[68] Santhoshsarang D M, Divya K, Telasang G, et al. Additively manufactured high-performance conformally cooled H13 tool steel die insert for pressure die casting. Transactions of the Indian National Academy of Engineering, 2021, 6(4): 1037–1048.
[69] Lu Y, Ripplinger K, Huang X, et al. A new fatigue life model for thermally-induced cracking in H13 steel dies for die casting. Journal of Materials Processing Technology, 2019, 271: 444–454.

[70] Ding R, Yang H, Li S, et al. Failure analysis of H13 steel die for high pressure die casting Al alloy. Engineering Failure Analysis, 2021, 124: 105330.
[71] Liu Y, Zhang Y, Liu W, et al. Enhanced mechanical properties and thermal conductivity of high-pressure die-cast AlMg6Si2MnZr alloy by controlling the externally solidified crystals. Journal of Materials Processing Technology, 2022, 306: 117645.
[72] Zabala B, Igartua A, Scarpis V, et al. Multiparametric study of Leidenfrost point and wettability of lubricants on high-pressure die-casting dies. International Journal of Thermal Sciences, 2018, 125: 66–73.
[73] Shaat M, Zheng Y. Fluidity and phase transitions of water in hydrophobic and hydrophilic nanotubes. Scientific Reports, 2019, 9(1): 5689.
[74] Mirbagheri S M H, Shrinparvar M, Ashory H, et al. Simulation of surface roughness on the flow pattern in the casting process. Materials & Design, 2004, 25(8): 655–661.
[75] Bai Z, Wu X. Effects of soldering and wear of die-casting die during ejection: Surface roughness and casting temperature. Engineering Failure Analysis, 2023, 151: 107383.
[76] Di Sabatino M, Arnberg L. Castability of aluminium alloys. Transactions of the Indian Institute of Metals, 2009, 62(4): 321–325.
[77] Brezina M, Kondic V. Flow phenomena in investment casting. British Foundryman, 1973, 66: 337–348.
[78] Wu K T, Hishamunda J B, Chen D T N, et al. Transition from turbulent to coherent flows in confined three-dimensional active fluids. Science, 2017, 355(6331): eaal1979.
[79] Lavernia E J, Srivatsan T S. The rapid solidification processing of materials: science, principles, technology, advances, and applications. Journal of Materials Science, 2010, 45(2): 287–325.
[80] Haga T, Imamura S, Fuse H. Fluidity investigation of pure Al and Al-Si alloys. Materials, 2021, 14(18): 5372.
[81] Aghion E, Moscovitch N, Arnon A. The correlation between wall thickness and properties of HPDC magnesium alloys. Materials Science and Engineering: A, 2007, 447(1–2): 341–346.
[82] Kim C W, Kim Y C, Kim J H, et al. Effect of alloying elements on the thermal conductivity and casting characteristics of aluminum alloys in high pressure die casting. Korean Journal of Metals and Materials, 2018, 56(11): 805–812.
[83] Han Q, Xu H. Fluidity of alloys under high pressure die casting conditions. Scripta Materialia, 2005, 53(1): 7–10.
[84] Otarawanna S, Gourlay C M, Laukli H I, et al. The thickness of defect bands in high-pressure die castings. Materials Characterization, 2009, 60(12): 1432–1441.
[85] Akamatsu S, Plapp M. Eutectic and peritectic solidification patterns. Current Opinion in Solid State and Materials Science, 2016, 20(1): 46–54.
[86] Hutt J E C, StJohn D H, Hogan L, et al. Equiaxed solidification of Al-Si alloys. Materials Science and Technology, 1999, 15(5): 495–500.
[87] Dahle A K, Karlsen S, Arnberg L. Effect of grain refinement on the fluidity of some binary Al-Cu and Al-Mg alloys. International Journal of Cast Metals Research, 1996, 9(2): 103–112.
[88] Cai Q, Mendis C L, Chang I T, et al. Microstructure and mechanical properties of new die-cast quaternary Al-Cu-Si-Mg alloys. Materials Science and Engineering: A, 2021, 800: 140357.
[89] Smithells C J. Gases and metals. Lecture I. Journal of the Royal Society of Arts, 1938, 86(4472): 936–949.
[90] MES Inc. Die casting aluminum selection guide. https://www.mesinc.net/wp-content/uploads/2025/03/Die-Casting-Aluminum-Selection-Guide.pdf, accessed January 10, 2025.
[91] Rheinfelden Alloys handbook. Primary aluminium casting alloys. Rheinfelden: Rheinfelden Alloys GmbH & Co. KG, 2016. https://rheinfelden-alloys.eu/wp-content/uploads/2017/01/Handbook-Die-Casting-Aluminium-Alloys_RHEINFELDEN-ALLOYS_2016_EN.pdf.
[92] Huang Y, Li W, Wang K. Investigation on fluidity, anodizing and tensile properties of Al-Mn alloys for application in thin-wall cast components. Materials Research Express, 2019, 6(7): 076571.
[93] Costa S C, Kenisarin M. A review of metallic materials for latent heat thermal energy storage: Thermophysical properties, applications, and challenges. Renewable and Sustainable Energy Reviews, 2022, 154: 111812.
[94] Ragone D V, Adams C M, Taylor H F. A new method for determining the effect of solidification range on fluidity. Transactions AFS, 1956, 64: 653–657.
[95] Cho Y H, Kim H W, Lee J M, et al. A new approach to the design of a low Si-added Al-Si casting alloy for optimising thermal conductivity and fluidity. Journal of Materials Science, 2015, 50(22): 7271–7281.
[96] Yıldırım M, Özyürek D. The effects of Mg amount on the microstructure and mechanical properties of Al-Si-Mg alloys. Materials & Design, 2013, 51: 767–774.
[97] Fortini A, Merlin M, Fabbri E, et al. On the influence of Mn and Mg additions on tensile properties, microstructure and quality index of the A356 aluminum foundry alloy. Procedia Structural Integrity, 2016, 2: 2238–2245.
[98] Vatankhah B R. Casting fluidity, viscosity, microstructure and tensile properties of aluminum matrix composites with different Mg_2Si contents. Rare Metals, 2022, 41(8): 2767–2776.
[99] Barenji R V. Effect of reinforcement amount, mold temperature, superheat, and mold thickness on fluidity of in-situ Al-Mg_2Si composites. China Foundry, 2018, 15(1): 66–74.
[100] Heidarzadeh A, Emamy M, Rahimzadeh A, et al. The Effect of copper addition on the fluidity and viscosity of an Al-Mg-Si alloy. Journal of Materials Engineering and Performance, 2014, 23(2): 469–476.
[101] Li Y, Li H, Katgerman L, et al. Recent advances in hot tearing during casting of aluminium alloys. Progress in Materials Science, 2021, 117: 100741.
[102] Jiao X Y, Liu C F, Guo Z P, et al. On the characterization of primary iron-rich phase in a high-pressure die-cast hypoeutectic Al-Si alloy. Journal of Alloys and Compounds, 2021, 862: 158580.
[103] Taghaddos E, Hejazi M M, Taghiabadi R, et al. Effect of iron-intermetallics on the fluidity of 413 aluminum alloy. Journal of Alloys and Compounds, 2009, 468(1–2): 539–545.
[104] Jiao X Y, Liu Y X, Wang J, et al. The microstructure characteristics and fracture behavior of the polyhedral primary iron-rich phase and plate-shaped eutectic iron-rich phase in a high-pressure die-cast AlSi10MnMg alloy. Journal of Materials Science & Technology, 2023, 140: 201–209.
[105] Wang D, Zhang X, Xu S, et al. Improvement of mechanical properties in micro-alloying Al-Si-Mg-Zn cast alloy. Materials Letters, 2021, 283: 128810.
[106] Hu B, Quan B, Li D, et al. Solid solution strengthening mechanism in high pressure die casting Al-Ce-Mg alloys. Materials Science and Engineering: A, 2021, 812: 141109.
[107] Mahmoud M G, Zedan Y, Samuel A M, et al. The use of rare earth metals in Al-Si-Cu casting alloys. International Journal of Metalcasting, 2022, 16(2): 535–552.
[108] Kwon Y D, Lee Z H. The effect of grain refining and oxide inclusion on the fluidity of Al-4.5Cu-0.6Mn and A356 alloys. Materials Science and Engineering: A, 2003, 360(1–2): 372–376.
[109] Dahle A K, Tøndel P A, Paradies C J, et al. Effect of grain refinement on the fluidity of two commercial Al-Si foundry alloys. Metallurgical and Materials Transactions: A, 1996, 27(8): 2305–2313.

[110] Ma Y, Liu Y, Wang M. Microstructures and corrosion resistances of hypoeutectic Al-6.5 Si-0.45 Mg casting alloy with addition of Sc and Zr. Materials Chemistry and Physics, 2022, 276: 125321.
[111] Mousavi M G, Cross C E, Grong Ø. Effect of scandium and titanium-boron on grain refinement and hot cracking of aluminium alloy 7108. Science and Technology of Welding and Joining, 1999, 4(6): 381–388.
[112] Prach O, Trudonoshyn O, Randelzhofer P, et al. Multi-alloying effect of Sc, Zr, Cr on the Al-Mg-Si-Mn high-pressure die casting alloys. Materials Characterization, 2020, 168: 110537.
[113] Prukkanon W, Srisukhumbowornchai N, Limmaneevichitr C. Influence of Sc modification on the fluidity of an A356 aluminum alloy. Journal of Alloys and Compounds, 2009, 487(1–2): 453–457.
[114] Çolak M, Kayikci R, Dispinar D. Influence of different cross sections on fluidity characteristics of A356. Transactions of the Indian Institute of Metals, 2015, 68(2): 275–281.
[115] Kim J M, Park B K, Jun J H, et al. Die-casting capabilities of heat resistant Mg-Al-Ca alloys. Trans Tech Publications, 2005: 424–427.
[116] Yim C D, You B S, Jang R S, et al. Effects of melt temperature and mold preheating temperature on the fluidity of Ca containing AZ31 alloys. Journal of Materials Science, 2006, 41(8): 2347–2350.
[117] Veldman N L, Dahle A K, StJohn D H, et al. Dendrite coherency of Al-Si-Cu alloys. Metallurgical and Materials Transactions: A, 2001, 32(1): 147–155.
[118] Hegde S, Prabhu K N. Modification of eutectic silicon in Al-Si alloys. Journal of Materials Science, 2008, 43(9): 3009–3027.
[119] Mollard F R, Flemings M C, Niyama E F. Aluminum fluidity in casting. JOM, 1987, 39(11): 34–34.
[120] Yang L, Li W, Du J, et al. Effect of Si and Ni contents on the fluidity of Al-Ni-Si alloys evaluated by using thermal analysis. Thermochimica Acta, 2016, 645: 7–15.
[121] Niu G, Mao J, Wang J. Effect of Ce Addition on fluidity of casting aluminum alloy A356. Metallurgical and Materials Transactions: A, 2019, 50(12): 5935–5944.
[122] Yang L, Li W, Du J, et al. Effect of Si and Ni contents on the fluidity of Al-Ni-Si alloys evaluated by using thermal analysis. Thermochimica Acta, 2016, 645: 7–15.
[123] Zhao Z, Li D, Yan X, et al. Insights into the dual effects of Ti on the grain refinement and mechanical properties of hypoeutectic Al-Si alloys. Journal of Materials Science & Technology, 2024, 189: 44–59.
[124] Cleary P W, Ha J, Prakash M, et al. Short shots and industrial case studies: Understanding fluid flow and solidification in high pressure die casting. Applied Mathematical Modelling, 2010, 34(8): 2018–2033.
[125] Zhu B W, Li L X, Liu X, et al. Effect of viscosity measurement method to simulate high pressure die casting of thin-wall AlSi10MnMg alloy castings. Journal of Materials Engineering and Performance, 2015, 24(12): 5032–5036.
[126] Kolsgaard A. Casting characteristics of SiC particulate reinforced $AlSi_7Mg$ aluminium matrix composites. Doctoral Dissertation, Norwegian Institute of Technology, Trondheim, 1993.
[127] Sahoo K L, Sivaramakrishnan C S. Some studies on Al-8.3Fe-0.8V-0.9Si alloy for near net shape casting. Journal of Materials Processing Technology, 2003, 135(2–3): 253–257.
[128] Yang W, Yang X, Ji S. Melt superheating on the microstructure and mechanical properties of diecast Al-Mg-Si-Mn alloy. Metals and Materials International, 2015, 21(2): 382–390.
[129] Lloyd D J. Particle reinforced aluminium and magnesium matrix composites. International Materials Reviews, 1994, 39(1): 1–23.
[130] Lee S L, Tzong R Y. Latent heat method for solidification process of a binary alloy system. International Journal of Heat and Mass Transfer, 1995, 38(7): 1237–1247.
[131] Homa M, Sobczak N. Measurements of temperature and heat of phase transformation of pure silicon by using differential scanning calorimetry. Journal of Thermal Analysis and Calorimetry, 2019, 138(6): 4215–4221.
[132] Đjurdjević M B, Jovanović V, Komatina M, et al. The specificity of determining the latent heat of solidification of cast hypoeutectic AlSiCu alloys using the DSC method. Materials, 2024, 17(17): 4228.
[133] Pan A, Wang J, Zhang X. Prediction of melting temperature and latent heat for low-melting metal PCMs. Rare Metal Materials and Engineering, 2016, 45(4): 874–880.
[134] Ben F, Olubambi P A. Thermo-Calc determination of phase diagram and thermodynamic properties of Ni-Al binary system. Materials Today: Proceedings, 2024, 105: 259–267.
[135] Li Z, Tan H, Lattanzi L, et al. On the possibility of replacing scheil-gulliver modeling with machine learning and neural network models. Solid State Phenomena, 2023, 347: 157–163.
[136] Lao X, Xu X, Wu J, et al. High-temperature alloy/honeycomb ceramic composite materials for solar thermal storage applications: Preparation and stability evaluation. Ceramics International, 2017, 43(5): 4583–4593.
[137] Harasima A. Molecular theory of surface tension. Advances in Chemical Physics, 1958, 1: 203–237.
[138] Moldover M R. Interfacial tension of fluids near critical points and two-scale-factor universality. Physical Review: A, 1985, 31(2): 1022.
[139] Ghatee M H, Zare M, Zolghadr A R, et al. Temperature dependence of viscosity and relation with the surface tension of ionic liquids. Fluid Phase Equilibria, 2010, 291(2): 188–194.
[140] Campbell J. Review of fluidity concepts in casting. Cast Metals, 1995, 7(4): 227–237.
[141] Morimoto S, Ohnishi N, Okada S. Development of a low-pressure die casting process for improved soundness of aluminum castings. AFS Transactions, 1987, 95: 39–46.
[142] Djurdjevic M B, Manasijevic S, Patarić A, et al. Challenges by latent heat calculation – Competition among analytical and computational methods. International Communications in Heat and Mass Transfer, 2024, 157: 107704.
[143] Arrhenius S. On the internal friction of dilute aqueous solutions. Journal of Physical Chemistry, 1887, 1(1): 285–298. (In German)
[144] Atkinson H V. Modelling the semisolid processing of metallic alloys. Progress in Materials Science, 2005, 50(3): 341–412.
[145] Fu Y, Li H, Tang K, et al. Melt viscosity of light alloys: Progress and challenges. Journal of Materials Science & Technology, 2024, 183: 72–88.
[146] Zhang F, Du Y, Liu S, et al. Modeling of the viscosity in the Al-Cu-Mg-Si system: Database construction. Calphad, 2015, 49: 79–86.
[147] Liu T Y, Atkinson H V, Kapranos P, et al. Rapid compression of aluminum alloys and its relationship to thixoformability. Metallurgical and Materials Transactions: A, 2003, 34(7): 1545–1554.
[148] Flemings M C. Solidification processing. Metallurgical Transactions, 1974, 5(10): 2121–2134.
[149] Hoyas S, Oberlack M, Alcántara-Ávila F, et al. Wall turbulence at high friction Reynolds numbers. Physical Review Fluids, 2022, 7(1): 014602.
[150] Vinarcik E J. High integrity die casting processes. John Wiley & Sons, 2002.

[151] Sigworth G K, Donahue R J. The metallurgy of aluminum alloys for structural high-pressure die castings. International Journal of Metalcasting, 2021, 15(3): 1031–1046.
[152] Harker J H, Backhurst J R, Richardson J F. Chemical Engineering, Volume 2: 2. Elsevier, 2013.
[153] Fiore M, Koloszar L, Fare C, et al. Physics-constrained machine learning for thermal turbulence modelling at low Prandtl numbers. International Journal of Heat and Mass Transfer, 2022, 194: 122998.
[154] Blass A, Tabak P, Verzicco R, et al. The effect of Prandtl number on turbulent sheared thermal convection. Journal of Fluid Mechanics, 2021, 910: A37.
[155] Cengel Y A, Ghajar A J. Internal forced convection. Heat Transfer, A: Practical Approach, 2nd ed. USA: McGraw-Hill, 2002: 419–458.
[156] Salunkhe P B, Shembekar P S. A review on effect of phase change material encapsulation on the thermal performance of a system. Renewable and Sustainable Energy Reviews, 2012, 16(8): 5603–5616.
[157] Kurotani Y, Tanaka H. A novel physical mechanism of liquid flow slippage on a solid surface. Science Advances, 2020, 6(13): eaaz0504.
[158] Zou G, Chai Y, Shen Q, et al. Analysis of the fluidity and hot tearing susceptibility of AlSi3.5Mg0.5Cu0.4 and A356 aluminum alloys. International Journal of Metalcasting, 2022, 16(2): 909–923.
[159] Di Sabatino M, Arnberg L. A review on the fluidity of Al based alloys. Metallurgical Science and Tecnology, 2004, 22(1). https://api.semanticscholar.org/CorpusID:55784742.
[160] Solsona M, Keizer H, de Boer H L, et al. Trajectory deflection of spinning magnetic microparticles: The Magnus effect at the microscale. Journal of Applied Physics, 2020, 127(19).
[161] Vandersluis E, Ravindran C. Comparison of measurement methods for secondary dendrite arm spacing. Metallography, Microstructure, Analysis, 2017, 6: 89–94.
[162] Cho J I, Kim C W. The relationship between dendrite arm spacing and cooling rate of Al-Si casting alloys in high pressure die casting. International Journal of Metalcasting, 2014, 8(1): 49–55.
[163] Jiao X Y, Liu C F, Guo Z P, et al. The characterization of Fe-rich phases in a high-pressure die cast hypoeutectic aluminum-silicon alloy. Journal of Materials Science & Technology, 2020, 51: 54–62.
[164] Gourlay C M, Dahle A K, Laukli H I. Segregation band formation in Al-Si die castings. Metallurgical and Materials Transactions: A, 2004, 35(9): 2881–2891.
[165] Chen J, Xu X, Zhou J, et al. Interfacial thermal resistance: Past, present, and future. Reviews of Modern Physics, 2022, 94(2): 025002.
[166] Kang B K, Sohn I. Effects of Cu and Si contents on the fluidity, hot tearing, and mechanical properties of Al-Cu-Si alloys. Metallurgical and Materials Transactions: A, 2018, 49(10): 5137–5145.
[167] Sharma D G R, Krishnan M, Ravindran C. Determination of the rate of latent heat liberation in binary alloys. Materials Characterization, 2000, 44(3): 309–320.
[168] Cinkilic E, Ridgeway C D, Yan X, et al. A formation map of iron-containing intermetallic phases in recycled cast aluminum alloys. Metallurgical and Materials Transactions: A, 2019, 50(12): 5945–5956.
[169] Ershkov S V, Prosviryakov E Y, Burmasheva N V, et al. Towards understanding the algorithms for solving the Navier-Stokes equations. Fluid Dynamics Research, 2021, 53(4): 044501.
[170] Higuera F J, Liñán A. Choking conditions for nonuniform viscous flows. Physics of Fluids, A: Fluid Dynamics, 1993, 5(3): 768–770.
[171] Pivkin I V, Karniadakis G E. Controlling density fluctuations in wall-bounded dissipative particle dynamics systems. Physical Review Letters, 2006, 96(20): 206001.
[172] Dyre J C. Solidity of viscous liquids. IV. Density fluctuations. Physical Review, E: Statistical, Nonlinear, and Soft Matter Physics, 2006, 74(2): 021502.
[173] Li X, Xiong S M, Guo Z. On the tensile failure induced by defect band in high pressure die casting of AM60B magnesium alloy. Materials Science and Engineering: A, 2016, 674: 687–695.
[174] Bhagavath S, Gong Z, Wigger T, et al. Mechanisms of gas and shrinkage porosity formation in solidifying shear bands. Journal of Materials Processing Technology, 2022, 299: 117338.
[175] Dietterich T G. Machine learning. Annual Review of Computer Science, 1990, 4(1): 255–306.
[176] Yao X. Evolving artificial neural networks. In: Proceedings of the IEEE, 1999, 87(9): 1423–1447.
[177] Juang P S H, Huang Y N, Kafando D A. Using machine learning to establish the relationship between die casting parameters and the casting quality. In: Proceedings of the 7th World Congress on Mechanical, Chemical, and Material Engineering (MCM'21), 2021, paper no. ICMIE 107.
[178] Duan Z, Chen W, Pei X, et al. A multimodal data-driven design of low pressure die casting gating system for aluminum alloy cabin. Journal of Materials Research and Technology, 2023, 27: 2723–2736.
[179] Wang X, Ding Z, Li S, et al. Computation method for mechanical performances of die-cast aluminum alloys based on non-uniform material properties. Materials Today Communications, 2024, 40: 109683.
[180] Ziabari A, Singanallur V, Snow Z, et al. Enabling rapid X-ray CT characterisation for additive manufacturing using CAD models and deep learning-based reconstruction. Preprint 2022-07-14, https://doi.org/10.21203/rs.3.rs-1808982/v1.
[181] Stempfle T, Mangos C, Feldmann S, et al. Artificial intelligence-based error detection and adaption of shot curve parameters in the hot chamber high-pressure die casting process. In: Proc. 2024 8th International Conference on Robotics and Automation Sciences (ICRAS), Tokyo, Japan: IEEE, 2024: 140–150.
[182] Shao Y, Li H, Gu X, et al. Distributed graph neural network training: A survey. ACM Computing Surveys, 2024, 56(8): 1–39.
[183] Van Eck N, Waltman L. Software survey: VOSviewer, a computer program for bibliometric mapping. Scientometrics, 2010, 84(2): 523–538.
[184] Jagadeesan S, Janardhan M, Singh B, et al. Machine learning model to reduce the various defects on die casting process. In: Proc. 2023 3rd Asian Conference on Innovation in Technology (ASIANCON), Ravet IN, India: IEEE, 2023: 1–5.
[185] Huang S J, Adityawardhana Y, Sanjaya J. Predicting mechanical properties of magnesium matrix composites with regression models by machine learning. Journal of Composites Science, 2023, 7(9): 347.
[186] Hu M, Tan Q, Knibbe R, et al. Designing unique and high-performance Al alloys via machine learning: Mitigating data bias through active learning. Computational Materials Science, 2024, 244: 113204.
[187] Murakami Y, Furushima R, Shiga K, et al. Mechanical property prediction of aluminium alloys with varied silicon content using deep learning. Acta Materialia, 2025, 286. https://doi.org/10.1016/j.actamat.2024.120683.
[188] Chen Y, Wang S, Xiong J, et al. Identifying facile material descriptors for Charpy impact toughness in low-alloy steel via machine learning. Journal of Materials Science & Technology, 2023, 132: 213–222.

[189] Krimpenis A, Benardos P G, Vosniakos G C, et al. Simulation-based selection of optimum pressure die-casting process parameters using neural nets and genetic algorithms. The International Journal of Advanced Manufacturing Technology, 2006, 27(5–6): 509–517.
[190] Wu Z, Wu Y, Zhang E. Study on die casting speed control based on neural network. In: Proc. 2020 International Conference on Communications, Information System and Computer Engineering (CISCE), Kuala Lumpur, Malaysia: IEEE, 2020: 407–410.
[191] Park S, Youm S. Establish a machine learning based model for optimal casting conditions management of small and medium sized die casting manufacturers. Scientific Reports, 2023, 13(1): 17163.
[192] Uyan T C, Otto K, Silva M S, et al. Industry 4.0 foundry data management and supervised machine learning in low-pressure die casting quality improvement. International Journal of Metalcasting, 2023, 17(1): 414–429.
[193] Frayman Y, Zheng H, Nahavandi S, et al. Machine vision system for automatic inspection of surface defects in aluminum die casting. Journal of Advanced Computational Intelligence and Intelligent Informatics, 2006, 10(3): 281–286.
[194] Tao C, Cheng X, Xu F, et al. Optimization and analysis of die-casting Al alloy solid solution process based on response surface model and NSGA-2 algorithm. Materials Express, 2024, 14(2): 329–338.
[195] Cica D, Kramar D. Intelligent process modeling and optimization of porosity formation in high-pressure die casting. International Journal of Metalcasting, 2018, 12(4): 814–824.
[196] Aksoy B, Koru M. Estimation of casting mold interfacial heat transfer coefficient in pressure die casting process by artificial intelligence methods. Arabian Journal for Science and Engineering, 2020, 45(11): 8969–8980.
[197] Zuo D, Lu Y. Design of amorphous alloy composition and optimization of vacuum die casting process parameters based on Co-evolutionary algorithm. IEEE Access, 2024, 12: 123883–123896.
[198] Gupta A K, Kumar S, Chandna P, et al. Optimization of process parameters during pressure die casting of A380: A silicon-based aluminium alloy using GA & fuzzy methodology. Silicon, 2021, 13(8): 2429–2443.
[199] Kittur J K, Manjunath P G C, Parappagoudar M B. Modeling of pressure die casting process: An artificial intelligence approach. International Journal of Metalcasting, 2016, 10(1): 70–87.
[200] Yarlagadda P K D V, Cheng W C E. A neural network system for the prediction of process parameters in pressure die casting. Journal of Materials Processing Technology, 1999, 89–90: 583–590.
[201] Tsoukalas V D. Optimization of porosity formation in AlSi9Cu3 pressure die castings using genetic algorithm analysis. Materials & Design, 2008, 29(10): 2027–2033.
[202] Chiang K T, Liu N M, Chou C C. Machining parameters optimization on the die casting process of magnesium alloy using the grey-based fuzzy algorithm. The International Journal of Advanced Manufacturing Technology, 2008, 38(3–4): 229–237.
[203] Xu P, Ji X, Li M, et al. Small data machine learning in materials science. npj Computational Materials, 2023, 9(1): 42.
[204] Schmidt J, Marques M R G, Botti S, et al. Recent advances and applications of machine learning in solid-state materials science. npj Computational Materials, 2019, 5(1): 83.
[205] Li H, Li X, Li Y, et al. Machine learning assisted design of aluminum-lithium alloy with high specific modulus and specific strength. Materials & Design, 2023, 225: 111483.
[206] Zhuang X, Antonov S, Li W, et al. Alloying effects and effective alloy design of high-Cr CoNi-based superalloys via a high-throughput experiments and machine learning framework. Acta Materialia, 2023, 243: 118525.
[207] Benesty J, Chen J, Huang Y, et al. Pearson correlation coefficient//Noise reduction in speech processing. Springer, 2009: 1–4.
[208] Chen X W, Jeong J C. Enhanced recursive feature elimination. In: Proc. Sixth international conference on machine learning and applications (ICMLA 2007), IEEE, 2007: 429–435.
[209] Hocking R R, Leslie R N. Selection of the best subset in regression analysis. Technometrics, 1967, 9(4): 531–540.
[210] Shahane S, Aluru N, Ferreira P, et al. Optimization of solidification in die casting using numerical simulations and machine learning. Journal of Manufacturing Processes, 2020, 51: 130–141.
[211] Parlak İ E, Emel E. Deep learning-based detection of aluminum casting defects and their types. Engineering Applications of Artificial Intelligence, 2023, 118: 105636.
[212] Bhat V, Balikai V G, Revankar P P, et al. A review on quality assurance in aluminium die casting through deep learning-based defect detection. E3S Web of Conferences, 2024, 556: 01010.
[213] Dai H, MacBeth C. Effects of learning parameters on learning procedure and performance of a BPNN. Neural Networks, 1997, 10(8): 1505–1521.
[214] Rudack M, Rom M, Bruckmeier L, et al. Recurrent neural networks as virtual cavity pressure and temperature sensors in high-pressure die casting. The International Journal of Advanced Manufacturing Technology, 2024, 134(7/8): 3267.
[215] Holland J H. Genetic algorithms. Scientific American, 1992, 267(1): 66–73.
[216] Hassanat A, Almohammadi K, Alkafaween E, et al. Choosing mutation and crossover ratios for genetic algorithms – A review with a new dynamic approach. Information, 2019, 10(12): 390.
[217] Leondes C T. Fuzzy logic and expert systems applications. In: Fuzzy neural networks and their applications. Academic Press, San Diego, 1997.